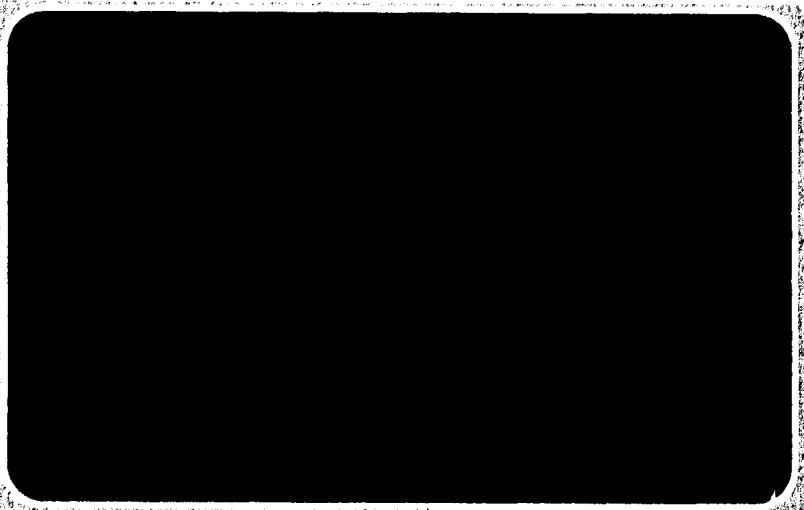

TU Delft

Lateral Escape Guidance Strategies for Microburst Windshear Encounters

Memorandum M-723

H.G. Visser

TU Delft
Delft University of Technology

Faculty of Aerospace Engineering

February 1996

Title : Lateral Escape Guidance Strategies for Microburst Windshear Encounters

Author(s) : H.G. Visser

Abstract : This study presents a preliminary evaluation of several candidate microburst escape guidance strategies, that rely on relatively short range forward-look sensing only. More specifically, three longitudinal guidance laws are developed and evaluated in combination with a single lateral guidance law. The sensor requirements that need to be satisfied in order to permit a practical implementation of the proposed guidance strategies are briefly examined as well. The simulated guidance solutions are then evaluated in terms of recovery-altitude performance and robustness to uncertainty in microburst size and strength. Based on a comparison with exact open-loop optimal solutions, altitude guidance emerged as the most promising longitudinal guidance strategy. The lateral escape strategy, though very simple, proved to be very effective. Several additions and refinements to the batch simulation are still required, before piloted simulations can take place. This report briefly outlines the missing elements, such as the to provide a framework for future research and development.

Keyword(s) : Guidance, minimax Chebyshev optimal control problems, dynamic inversion, windshear, microburst escape strategies, windshear detection systems.

Issue	1		
Date	February 1996		
Prepared	H.G. Visser		
Verified			
Approved	Th. van Holten	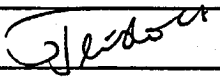	

Table of Contents

Nomenclature

a_{bx}, a_{by}, a_{bz}	-	Measured accelerations in body axes system
C_D, C_L	-	Aerodynamic coefficients
D	-	Drag force
E	-	Specific energy
g	-	Acceleration of gravity
h	-	Altitude
F	-	F-factor
F_{av}	-	Averaged measured F-factor
F_{thres}	-	Critical F-factor
K	-	Feedback gain
J	-	Performance index
L	-	Lift force, transformation matrix
r	-	Radial distance to microburst center
R_{look}	-	Detection range of the windshear sensor
S	-	Wing area
T	-	Thrust
t	-	Time
u	-	pseudo-control
V	-	Airspeed (TAS)
V_{IAS}	-	Indicated Airspeed (IAS)
W	-	Aircraft gross weight
W_h	-	Vertical windspeed
W_r	-	Radial (horizontal) windspeed
W_x, W_y	-	Horizonal windspeed components
x, y, z	-	Position coordinates of aircraft
x_c, y_c	-	Horizontal position coordinates of microburst center
Y	-	Side force
α	-	Angle-of-attack
β	-	Sideslip Angle
γ	-	Flight path angle
δ	-	Thrust inclination
η	-	Throttle setting
η_t	-	Throttle response
θ	-	Pitch angle
μ	-	Aerodynamic roll angle
ρ	-	Air density
τ	-	Time constant
ϕ	-	Roll angle
χ	-	Heading angle
χ_w	-	Horizontal wind direction
ψ	-	Yaw angle

Subscripts

0	- initial value
BW	- wind-to-body frame
c	- commanded value
EB	- body-to-Earth frame
EW	- wind-to-Earth frame
f	- final value
i	- inertial-axis quantity
max	- maximum value
ref	- reference value

Superscript

*	- optimal value

1. Introduction

Due to recent advances made in the area of forward looking windshear detection and warning systems, alert times of up to 90 seconds can be attained in an impending microburst encounter[1-6]. Clearly, alert times of this magnitude allow a pilot on final approach to totally avoid the microburst, simply by executing a go-around in a timely fashion. In the case of a moderate windshear hazard, a penetration landing might become a safe alternative procedure, provided that an adequate energy buffer can be build up before the high-shear region is entered. In view of the fairly large warning times offered by advanced detection and warning systems, one may wonder whether there is a real need for escape guidance strategies. However, as evidenced by some recent windshear accidents[7], a microburst may form and dissipate within a relatively short time span. Consequently, the need for guidance strategies is likely to remain even if advanced forward looking systems are employed.

A serious concern regarding forward looking airborne systems relates to affordability. In particular, the requirement that an airborne forward looking system or a system of sensors is to be capable of detecting both heavy ("wet") and light ("dry") precipitation microbursts appears to be a major cost driver. Another heavy requirement typically imposed to a forward-looking sensor or sensor system is that it must measure mean horizontal wind speeds every 150 to 300 m out to a range of 6 to 8 km along the flight path and a small sector (approx. 20°) on either side of the A/C with approximately 1 m/s accuracy[1]. Clearly, the required degree of sensor development represents a tradeoff between cost and performance.

In view of the high cost of current forward looking airborne sensor systems, it seems questionable whether such systems should be mandated for e.g. light regional aircraft (FAR 23). The development of ground-based windshear sensors (in combination with a data link) is likely to further fuel the reluctance within the air transport community to appropriate large investments in additional airborne equipment.

The aim of the present study is to develop near-optimal feedback escape strategies that rely on relatively short range forward looking sensing only. More specifically, lateral escape strategies in combination with more traditional longitudinal escape procedures are proposed to improve windshear recovery performance. The sensor requirements that need to be satisfied in order to permit a practical implementation of the proposed guidance strategies are briefly examined as well. It needs to be noted that the present study is only preliminary in nature and probably raises more questions than it answers. Nevertheless, since at this stage simulated closed-loop guidance solutions compare well with the "ideal" standards set by open-loop optimal control results, we feel that the preliminary study presented herein does provide a solid basis for future research.

Although in Ref.8 some preliminary results were already reported on closed-loop guidance strategies that closely approximate the open-loop optimal trajectories, the outcome of the more recent research effort presented in Ref.9 warranted a revision of the envisioned escape technique. In both Refs. 8 and 9, open-loop optimal escape maneuvers are established by solving a so-called ***minimax*** (or Chebyshev) optimal control problem. More specifically, for the abort landing the objective is to maximize the minimum altitude reached by an aircraft at any point along the trajectory, or, in other words, to minimize the peak value of the altitude drop (see Fig. 1) :

$$I^* = \min I = \min \left[\max_t \left(h_{ref} - h(t) \right) \right] \ , \quad 0 \le t \le t_f \ , \tag{1}$$

where h_{ref} is a constant reference altitude and $[0,t_f]$ is the fixed flight time interval. Based on a well-known result obtained using functional analysis, i.e.,

$$\lim_{k \to \infty} \left[\int_0^{t_f} \left(h_{ref} - h(t) \right)^{2k} dt \right]^{\frac{1}{2k}} = \max_t \left(h_{ref} - h(t) \right) \ , \tag{2}$$

the minimax criterion in Eq.(1) (Chebyshev performance index) is ***approximated*** by a Bolza performance index in Ref.8 :

$$J^* = \min J = \min \int_0^{t_f} (h_{ref} - h)^n \, dt \ , \tag{3}$$

where n is a large positive, even exponent. Note that for the best possible computational results, the reference altitude h_{ref} should be chosen as small as possible, but such that the right-hand side of Eq.(1) remains positive at all times. In Ref.8 the exponent in Eq.(3) was taken as n = 6 and the reference altitude taken as h_{ref} = 400 m.

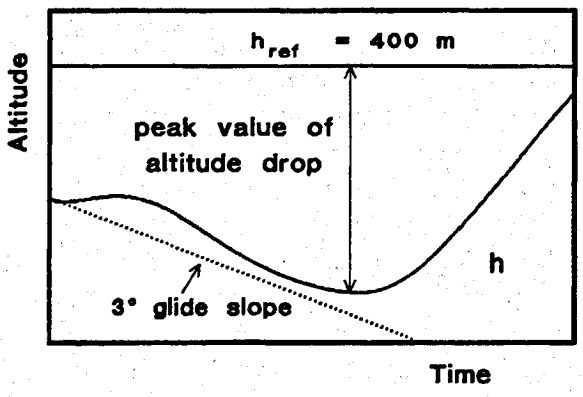

Figure 1 : Illustration of Performance Index

In contrast to the above performance index ***approximation***, a transformation technique which allows to solve the ***exact*** minimax problem (1) was applied in Ref.9. More specifically, the minimax problem was converted into an equivalent optimal control problem with state variable inequality constraints and the resulting Multi-Point-Boundary-Value-Problem (MPBVP) was subsequently solved using a multiple-shooting algorithm[10].

A comparison of solutions based on the Bolza performance index approximation ("Bolza solutions") with the solutions to the original minimax problem ("Chebyshev solutions") revealed not only a marked improvement in reducing the peak value of altitude drop, but perhaps even more significantly, also the overall longitudinal behavior is radically different. In Chebyshev solutions typically altitude is traded for airspeed in the initial phase of the encounter, such as to place the aircraft in a region of relatively low downdraft. Consequently, Chebyshev solutions generally no longer exhibit an initial climb in a lateral escape maneuver.

On the other hand, the difference in lateral behavior between Chebyshev and Bolza solutions is slight only. Generally speaking it can be observed that in the final stage of a lateral escape maneuver (i.e., in the after-shear region), an aircraft ends up flying along a horizontal wind radial. Based on this behavior, a closed-loop lateral escape strategy was developed in Ref.8. In particular, a constant pitch technique was examined in combination with a simple guidance law for the aerodynamic roll angle, which involves the feedback of the relative wind direction (i.e., the difference between the radial wind direction and the actual heading). This closed-loop guidance scheme approximates the open-loop optimal trajectories, relying on in situ wind information only. In the development of the lateral guidance law it was more or less implicitly assumed that the relative wind direction can be estimated onboard. This assumption will be critically reviewed herein.

The behavior of the simulated guidance solutions in Ref.8 showed a remarkable degree of agreement with the Bolza solutions. However, in view of earlier observations this also implies that the performance and behavior of the simulated guidance solutions do not closely approximate that of the Chebyshev solutions established in Ref.9. The main purpose of the present preliminary study therefore is to explore alternative guidance laws that offer improved performance. In particular, we seek to replace the constant pitch technique by an alternative longitudinal guidance law. As a matter of fact, two different candidate longitudinal strategies will be examined in addition to the constant pitch technique. The new longitudinal guidance laws have been derived based on dynamic inversion, along the lines of Ref.11. For lateral guidance the simple law as presented in Ref.8 has been retained here. For all three guidance concepts the benefits of forward-look sensing will be assessed relative to in situ measurement.

The organization of this report is as follows. Details concerning the simulation model are described in Chapter 2. Next, the characteristics of open-loop optimal Bolza and Chebyshev solutions are investigated for different locations of the microburst. In Chapter 4 the proposed longitudinal guidance laws will be derived. In Chapter 5 simulated closed-loop guidance trajectories are compared with open-loop optimal trajectories. Chapter 6 discusses some relevant aspects of windshear measurement. In the concluding Chapter the prospects for the proposed guidance laws are discussed.

2. Microburst encounter modeling

Using the relative wind-axes reference-frame defined in Ref.9, the equations of motion, describing the dynamics of a point-mass-modeled aircraft (including the effects of windshear) in the three-dimensional space can be written as:

$$\dot{x} = V\cos\gamma\cos\chi + W_x \tag{4}$$

$$\dot{y} = V\cos\gamma\sin\chi + W_y \tag{5}$$

$$\dot{h} = V\sin\gamma + W_h \tag{6}$$

$$\dot{E} = \frac{[T\cos(\alpha+\delta)\cos\beta - D\cos\beta + Y\sin\beta]V}{W} + \dot{W}_h - \frac{V}{g}[\dot{W}_x\cos\gamma\cos\chi + \dot{W}_y\cos\gamma\sin\chi + \dot{W}_h\sin\gamma] \tag{7}$$

$$\dot{\gamma} = \frac{g}{V}[\frac{L + T\sin(\alpha+\delta)}{W}\cos\mu + \frac{T\cos(\alpha+\delta)\sin\beta - D\sin\beta - Y\cos\beta}{W}\sin\mu - \cos\gamma] + \frac{1}{V}[\dot{W}_x\sin\gamma\cos\chi + \dot{W}_y\sin\gamma\sin\chi - \dot{W}_h\cos\gamma] \tag{8}$$

$$\dot{\chi} = \frac{g}{V\cos\gamma}[\frac{L+T\sin(\alpha+\delta)}{W}\sin\mu + \frac{-T\cos(\alpha+\delta)\sin\beta + D\sin\beta + Y\cos\beta}{W}\cos\mu] + \frac{1}{V\cos\gamma}[\dot{W}_x\sin\chi - \dot{W}_y\cos\chi] \tag{9}$$

$$\dot{\eta} = \frac{1}{\tau_T}[\eta_t - \eta] \tag{10}$$

where x, y and h are the position coordinates in a frame fixed to the ground, E is the specific energy, γ is the flight path angle, χ is the heading angle and η the throttle

response. The wind velocity vector has three components, viz., W_x, W_y and W_h. The above equations are on the basis of the following assumptions: (i) the wind flow field is steady, (ii) a flat non-rotating earth, and (iii) the aircraft weight is constant. The thrust T is assumed to have a fixed inclination δ relative to the zero-lift axis, but the thrust vector remains in the aircraft's plane of symmetry. The throttle response is modeled as a first-order lag with a time constant τ_T.

The above model is slightly more involved than that of Ref.9. As a matter fact, the model of Ref.9 can be obtained from the above model if the following additional assumptions are introduced, (1) a small angle approximation for the thrust vector components along and perpendicular to the airspeed vector, i.e., $\cos(\alpha+\delta) \approx 1 - \frac{1}{2}(\alpha+\delta)^2$ and $\sin(\alpha+\delta) \approx (\alpha+\delta)$, and (2) no sideslip (and sideforce), i.e., $\beta = 0$. The inclusion of the effect of sideslip in the present model is not really intended to enhance the simulation fidelity, but rather to facilitate the discussion of windshear estimation later in the report. Evidently, in any escape maneuver the aim is to keep sideslip close to zero and in the closed-loop guidance simulations it is therefore assumed that escape maneuvers are executed in a fully coordinated fashion ($\beta = 0$). It is important to note that the introduction of sideslip effects has forced us to resort to a slightly different notation in this report in comparison to Refs. 8 and 9. In particular, the variable β is used to denote the sideslip angle, rather than the relative thrust, as in Refs. 8 and 9.

The controls in the mathematical model are the same as in Refs. 8 and 9 :

(i) The throttle setting η_t constrained by:

$$0 \le \eta_t \le 1 \tag{11}$$

(ii) The aerodynamic roll angle μ which is limited by:

$$|\mu| \le \mu_{max} \tag{12}$$

(iii) The angle-of-attack α which is forced to remain within the range:

$$0 \le \alpha \le \alpha_{max} \tag{13}$$

The aerodynamic lift and drag forces (L and D) are modeled as functions of airspeed V, altitude h and the angle-of-attack α :

$$L = C_L(\alpha)\, qS = \left[L_0 + L_1\alpha + L_2(\alpha - \alpha_{ref})^2\right]\frac{1}{2}\rho V^2 S \tag{14}$$

$$D = C_D(\alpha) qS = \left[D_0 + D_1\alpha + D_2\alpha^2\right]\frac{1}{2}\rho V^2 S \tag{15}$$

Note that it is assumed here that both L and D are in the A/C plane of symmetry. The

sideforce Y is perpendicular to the A/C plane of symmetry and typically is a function of airspeed V, altitude h, the angle-of-attack α and sideslip angle β. Since $\beta = 0$ is assumed in the simulations, no effort has been to actually implement a model for the sideforce Y. The maximum thrust is assumed to be a function of airspeed only, i.e.:

$$T = \eta T_{max}(V) = \eta\left(T_0 + T_1 V + T_2 V^2\right) \tag{16}$$

The aircraft type used in the investigation is a Boeing 727. Details of the aerodynamic and thrust data for this aircraft type (in landing configuration) are given in Ref.8. Reference 8 also contains a description of the particular microburst wind field flow model (Soesman model) considered herein.

In view of the axisymmetric character of the microburst model, polar coordinates have been used to describe the flow field in a horizontal plane (see Fig. 2). The employed analytic flow field model computes the radial flow W_r as a function of the radial distance to the microburst center (r) and the downdraft W_h as a function of the radial distance r and the altitude h.

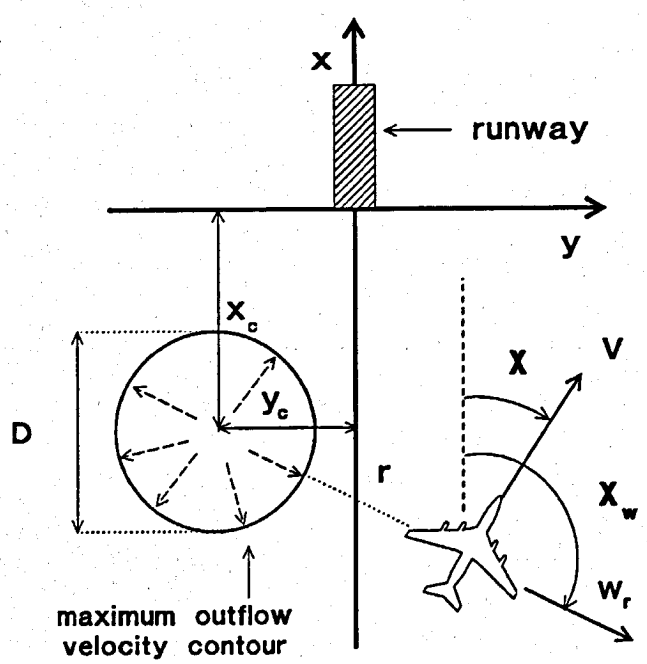

Figure 2 : Geometry of microburst encounter.

For a given aircraft position (x,y), it is readily clear from Figure 2 that the radial distance r from the microburst center (axis of symmetry) located at the point (x_c, y_c), can be computed from the relation:

$$r = \sqrt{(x - x_c)^2 + (y - y_c)^2} \tag{17}$$

Using polar coordinates, the horizontal wind components W_x and W_y can be related to the radial windvelocity W_r:

$$W_x = \cos\chi_w W_r(r) \;\; ; \;\; W_y = \sin\chi_w W_r(r) \;\; , \tag{18}$$

where χ_w is the direction of the radial wind velocity vector. The total derivatives of these wind velocity components satisfy the relations:

$$\dot{W}_x = \frac{\partial W_x}{\partial x}\dot{x} + \frac{\partial W_x}{\partial y}\dot{y} \;\; ; \;\; \dot{W}_y = \frac{\partial W_y}{\partial x}\dot{x} + \frac{\partial W_y}{\partial y}\dot{y} \tag{19}$$

$$\dot{W}_h = \frac{\partial W_h}{\partial x}\dot{x} + \frac{\partial W_h}{\partial y}\dot{y} + \frac{\partial W_h}{\partial h}\dot{h} \tag{20}$$

The wind terms in Eq.(7) that describe the windshear impact on aircraft specific energy parameter can be combined in a single characteristic parameter, called the F-factor:

$$F \triangleq \frac{(T - D)}{W} - \frac{\dot{E}}{V} \tag{21}$$

The F-factor can be interpreted as the loss or gain in available specific excess power due to the combined effect of downdraft and horizontal windshear. The F-factor therefore represents a direct measure of the degradation of an aircraft's potential climb gradient due to the windshear. Note that positive values of the F-factor indicate a performance decreasing situation. Since the F-factor is an important quantity in all proposed closed-loop guidance concepts, it needs to be estimated on board with reasonable accuracy. Another wind-related quantity important for (lateral) guidance is the wind-direction χ_w. Whether it is possible to estimate this quantity sufficiently accurate based on onboard measurements will be examined in Chapter 6. In the present simulation trials perfect information is assumed in the feedback schemes for forward-look sensors, as well as reactive systems. Forward-look detection is simulated by computing the wind vector and its spatial gradients at a single point located at a range R_{look} along the flight path vector. In the case of forward-look sensing the F-factor prediction is based on *advance* wind information, in combination with the *momentary* aircraft state.

3. Exact open-loop optimal solutions

In this Chapter the major findings established in Ref.9 are reiterated, primarily for the purpose of extracting the essential features of open-loop optimal trajectories. First, we formally restate the performance index that we seek to optimize. As already pointed out in the introduction, the objective in this study is to minimize the peak value of the altitude drop (h_{ref} - h), as expressed by the Chebyshev functional in Eq. (1). The Bolza functional that approximates the Chebyshev index is stated in Eq.(3). In normalized form it will be denoted here as J_1 :

$$J_1 = \int_0^{t_f} \left(1 - \frac{h}{h_{ref}}\right)^n dt \tag{22}$$

The original Chebyshev minimax performance index (1) will be denoted as J_2 :

$$J_2 = \left[\max_t \left(h_{ref} - h(t)\right) \right] , \quad 0 \le t \le t_f , \tag{23}$$

As outlined in Ref.9, specifying the Chebyshev index J_2 amounts to maximizing the minimum altitude constraint value h_{min}, associated with the artificially introduced state constraint :

$$h(t) \ge h_{min} \tag{24}$$

A third criterion considered in Ref.9 concerns the ***maximization*** of specific energy at termination :

$$J_3 = -E(t_f) \tag{25}$$

Obviously, the minus sign in Eq.(25) stems from the fact that we seek to minimize the performance index J_3. In order to permit a trade-off between the various performance criteria, the following "composite" index is formed :

$$\begin{aligned} \bar{J} &= \int_0^{t_f} \left(1 - \frac{h}{h_{ref}}\right)^n dt + K_1 \left[\max_t \left(h_{ref} - h(t)\right) \right] - K_2 E(t_f) \\ &= J_1 + K_1 J_2 + K_2 J_3 , \end{aligned} \tag{26}$$

where K_1, and K_2 are (positive) scaling factors. Also recall that a fixed flight time is considered (typically t_f is taken as 50 seconds). For the numerical computation of the optimal trajectories, a continuation process has been used, in which the two parameters K_1 and K_2 served as homotopy parameters. Obviously, the homotopy chain was started with $K_1 = K_2 = 0$, which corresponds to the previously established results involving the integral performance measure only[8]. In small steps the parameters K_1 and K_2 were gradually increased to large numbers. Note that the particular formulation of the performance index (26) precludes the specification of a "pure" Chebyshev performance measure. More specifically, for any finite value of K_1 there will always be some integral part J_1 in the composite performance measure (26). The numerical results in Ref.9 bear out that in practical terms the influence of the integral part can be made negligibly small, simply by specifying a very large value for K_1. As a matter of fact, the conclusion was drawn that a pure Chebyshev solution can already be fairly closely approximated by solving the optimal control problem for any value of K_1 in excess of 0.1 (assuming a zero value zero for K_2). Indeed, for large values of K_1 the integral part has influence on altitude behavior in the after-shear region only.

The same holds more or less true for the weight factor K_2. If a small weight factor K_2 is selected, the influence of the maximum specific energy part in the performance index is limited to the after-shear region only. In particular, the minimum altitude performance remains unaffected. Inclusion of a final specific energy term in the performance criterion is actually useful to improve overall trajectory behavior in the after-shear region, provided that a terminal boundary condition on flight path angle is imposed as well. It is conjectured that inclusion of this term helps to avoid existence and uniqueness in the aftershear region that would occur in a "pure" fixed final time Chebyshev optimization problem. This can be readily understood from the fact that the behavior of the controls is essentially irrelevant once the minimum altitude constraint limit is definitively departed. If a relatively large value is specified for K_2, the entire trajectory is influenced, in the sense that minimum altitude performance is sacrificed for the benefit of gaining specific energy. In practical terms K_2 can be increased until a trajectory is obtained for which the actually achieved minimum altitude matches the absolute safe minimum altitude. Note that maximizing final energy results in trajectories that are significantly different from the Chebyshev and Bolza solutions. Typically, relatively low angle-of-attack is employed throughout the maneuver and consequently the drop in airspeed in the high-shear region is significantly less than for the Chebyshev and Bolza solutions.

As already pointed out in Ref.12, some important lessons with regard to closed-loop guidance approximations can be learned from the above observations. Descending to a low altitude is clearly a beneficial procedure, in the sense that investing in kinetic energy results in a lower overall loss in specific energy than investing in potential energy. In open-loop Chebyshev solutions the actually achieved minimum altitude during the encounter is such that angle-of-attack reaches its limit at the end of the high-shear region. In contrast to an open-loop solution where perfect global wind information is available, in a real-world situation a fair degree of uncertainty with respect to the intensity and extent of the windshear is inevitable, even if advanced forward sensing technology is deployed. Consequently, when a microburst is encountered a pilot is generally unsure where and when the high-shear region will end, particularly in the case that an aircraft is equipped with a reactive windshear warning system only. If an aircraft descends below the "optimal" minimum altitude that is theoretically achievable in a Chebyshev solution, an additional survival capability is obtained, in the form of an "airspeed reserve". An airspeed

reserve makes an aircraft less vulnerable to uncertainties in microburst intensity and extent, by reducing the risk that the angle-of-attack limit is reached before the high-shear region is exited. As we will see in the sequel of this report, such an event may result in dramatic altitude loss. The largest airspeed reserve is obtained by descending to the lowest allowable altitude in terms of obstacle clearance. However, the question is, is it really wise to always descend to this minimum safe altitude? If this procedure is executed in a mild windshear, an aircraft may end up flying at high speed, close to the deck. Descending to an altitude level above the minimum safe altitude is then probably a safer procedure. In turn, opting for the latter technique obviously results in the question how to select the target altitude? If the target altitude is selected too high, the airspeed reserve may be too small and the aircraft runs out of steam before the high-shear region is exited. Only if the intensity and extent of the microburst can be estimated in advance, there appears to be some hope for the development of guidelines for selecting an appropriate target altitude. Alternatively, one could envision an adaptive guidance scheme that attempts to modify the control laws (e.g., the target altitude) based on continuously updated windshear predictions.

As discussed earlier, a guidance technique based on a constant target pitch angle results in trajectories that fairly closely approximate Bolza solutions. Another closed-loop guidance technique that has been proposed[4,11,12] is to direct the aircraft towards a specified target altitude. From the above analysis it can be concluded that this guidance technique more or less approximates Chebyshev/maximum final energy solutions. In Chapter 4 we shall derive similar guidance laws by extending the longitudinal analysis of Ref.4 to flight in three dimensions. As a matter of fact, two candidate longitudinal guidance strategies will be proposed in Chapter 4, one that schedules altitude and one that schedules climb rate. Obviously, by introducing these new guidance laws, we hope to achieve the same kind of minimum altitude performance improvement, as demonstrated by Chebyshev solutions in comparison with Bolza solutions.

Thus far, we have limited our discussion to one control variable, angle-of-attack. However, there are two more control variables, viz., throttle setting and aerodynamic roll angle. Angle-of-attack is mainly used to regulate the distribution of kinetic and potential energy. Obviously, full throttle is applied immediately when the pilot believes he is entering or is about to enter a microburst, such as to minimize the energy drain. The third control variable, aerodynamic roll angle, helps in achieving a positional advantage by cutting off the high-shear region. In other words, lateral maneuvering does not help to reduce the rate at which the energy is drained, but rather it reduces the timespan during which the aircraft is exposed to energy draining windshear. Reference 9 reveals that, in contrast to angle-of-attack, the aerodynamic roll angle behavior is not dramatically different for Bolza and Chebyshev solutions. This actually motivates us to retain the lateral guidance law already developed in Ref.8. However, note that this does not imply that longitudinal and lateral dynamics are not coupled. In particular for Bolza solutions, the angle-of-attack behavior can be significantly different for a lateral maneuver in comparison to a nonturning maneuver. For Chebyshev solutions these differences are less striking.

Although the exact open-loop optimal solutions presented in Ref.9 greatly contribute to the understanding of trajectory behavior, the numerical examples were by no means exhaustive, so that several unanswered questions remained. Several of these "loose ends" will be addressed here.

First of all, due to the large differences between the calculated Bolza solutions and Chebyshev solutions, one may question the validity of the Bolza performance index approximation for this particular problem, at least for the numerical values adopted thus far. For this reason, a new attempt has been to compute optimal Bolza solutions for higher values of the exponential n in the performance index (3). Indeed, we have been able to compute optimal trajectories with exponentials up to 16, albeit still with great difficulty. The following numerical example serves to illustrate the new results. Similar to the numerical examples in Refs.8 and 9, the following "standard" initial conditions (at which the escape procedure is commenced) have been assumed here :

$x(0) = x_0 = -2500$ m , $\quad y(0) = y_0 = 0$ m ,

$h(0) = h_0 = 131$ m , $\quad E(0) = E_0 = 384.326$ m ,

$\gamma(0) = \gamma_0 = -3°$, $\quad \chi(0) = \chi_0 = 0°$,

$\eta(0) = \eta_0 = 0.3334$

The microburst center is located on the runway centerline extension, 1500m ahead of the threshold. Moreover, the lateral maneuvers are executed with an aerodynamic roll angle limit of 10°. In Figs. 3 the results for the lateral escape trajectories are shown.

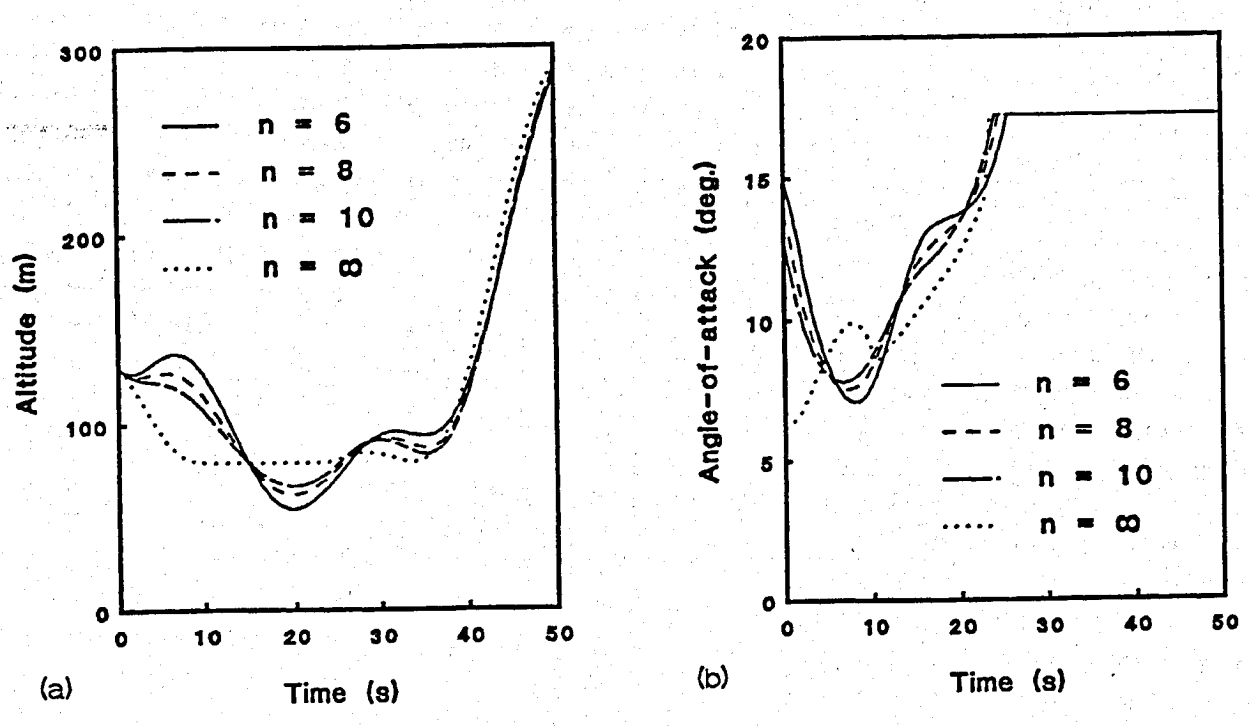

Figure 3 : Comparison of extremal solutions for various values of the exponential n in the integral performance index. Lateral maneuvering ($\mu_{max} = 10°$); $x_c = -1500$ m.

Three different values of the exponential n in the performance index J_1 are considered in Figure 3, viz., n = 6, 8, and 10. Additionally, the Chebyshev solution has been included. This solution has been labeled n = ∞ in Figure 3. It needs to be noted that solution n = ∞ is not really a "pure" Chebyshev solution, but for all practical purposes it can be considered as such.

From Figure 3a it is readily observed that the original Bolza performance index approximation J_1, featuring n = 6, produces rather unsatisfactory results in terms of minimum altitude performance. Increasing the power n from 6 to 8 already results in a vast improvement, despite the fact that the angle-of-attack behavior is not significantly affected. Increasing the power n even further, from 8 to 10, raises the minimum altitude to a higher level. At the same time, we start to see the initial climb disappearing. A comparison of the Bolza solution with n = 10 with the Chebyshev solution makes clear that the minimum altitude performance is still not really closely approximated. As mentioned before, the most striking difference between the Bolza solutions and the Chebyshev solution concerns the angle-of-attack behavior in the initial phase of the escape, resulting in an immediate descend rather than a climb. It is recalled that the present results actually resemble the results obtained previously in Ref.9 (n = 6), for the same example, but now for various values of the weight factor K_1. For the sake of clarity, the results presented in Ref.9 (i.e., Figure 5) are summarized here in Figure 4. Note that the solution K_1 = 0.025 in Figure 4 is in remarkable agreement with the solution for the power n = 10 in Figure 3, excepting the brief period of horizontal flight in Figure 4. Comparing the solutions for K_1 = 0.025 and K_1 = 25 in Figure 4, it can be readily concluded that, while angle-of-attack and altitude behavior are rather different, the difference in the minimum altitude is not so large. This forms perhaps the best explanation of the fact that the target pitch technique and the target altitude guidance approach did not demonstrate statistically significant performance differences in the piloted simulation study of Ref.4.

Another problem relates to the selection of initial conditions. The initial condition represents the aircraft state at the initiation of the escape maneuver. Up to now the above standard set of initial conditions has been considered in most numerical experiments. These initial values correspond to a situation in which an aircraft would fly during a stabilized approach (V = 70.5 m/s) without winds or windshear, when the aircraft is still 2500 m from the runway threshold. In Refs.8 and 9 it was already acknowledged that in the presence of winds, the required values for γ_0 and η_0 will be different. Indeed, an alternative way to generate the initial conditions is to assume a set of initial conditions in terms of specified inertial-axis quantities. The inertial-axis variables are easily related to the wind-axis variables :

$$V_i = \sqrt{(V\cos\gamma\cos\chi + W_x)^2 + (V\cos\gamma\sin\chi + W_y)^2 + (V\sin\gamma + W_h)^2}$$
$$= \sqrt{(V\cos\gamma)^2 + W_r^2 + 2V\cos\gamma W_r\cos(\chi - \chi_w) + (V\sin\gamma + W_h)^2} \qquad (27)$$

$$\tan\gamma_i = \frac{V\sin\gamma + W_h}{\sqrt{(V\cos\gamma\cos\chi + W_x)^2 + (V\cos\gamma\sin\chi + W_y)^2}}$$

$$= \frac{V\sin\gamma + W_h}{\sqrt{(V\cos\gamma)^2 + W_r^2 + 2V\cos\gamma W_r\cos(\chi - \chi_w)}} \qquad (28)$$

$$\tan\chi_i = \frac{V\cos\gamma\sin\chi + W_y}{V\cos\gamma\cos\chi + W_x} \qquad (29)$$

In case of a symmetric encounter in headwind (χ - χ_w = ± 180°), the relations (27) and (28) simplify to :

$$V_i = \sqrt{(V\cos\gamma - W_r)^2 + (V\sin\gamma + W_h)^2} \qquad (30)$$

$$\tan\gamma_i = \frac{V\sin\gamma + W_h}{V\cos\gamma - W_r} \qquad (31)$$

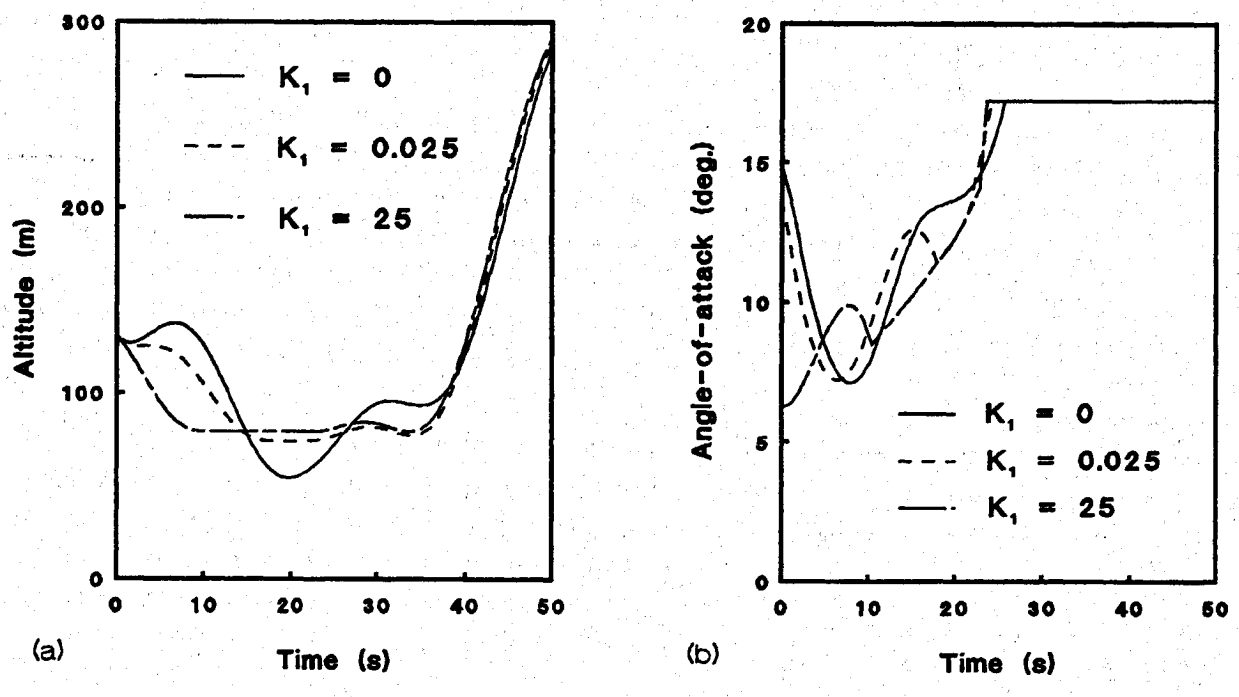

Figure 4 : Comparison of extremal solutions for various values of K_1. Lateral maneuvering, with μ_{max} = 10°; the weight factor K_2 = 0.

In stead of specifying the initial airspeed V_0 and initial flight path angle γ_0, the corresponding inertial-axis quantities could be specified :

$$V_i(0) = 70.5 \text{ m/s} \qquad \gamma_i(0) = -3°$$

From Eqs.(30) and (31) it is clear that a problem arises if trajectories with different locations of the microburst are considered. A different location of the microburst leads to a different wind condition at the initial aircraft position, which in turn leads to different values of V_0 and γ_0. Moreover, the initial throttle setting η_0 will be different for each different microburst location (assuming a stabilized approach). In view of the severe wind conditions that may exist in the proximity of a microburst, the difference between the wind-axis and inertial-axis quantities can be considerable. Substitution of the "standard" wind-axis initial values and windspeeds at the initial point (generated by a microburst located at $x_c = -1500$ m, $y_c = 0$ m) in Eqs. (30) and (31) results in :

$$V_i(0) = 52.55 \text{ m/s} \qquad \gamma_i(0) = -6.36° \qquad (W_r = 18.18 \text{ m/s}; W_h = -2.14 \text{ m/s})$$

In other words, a rather low groundspeed and a rather high rate of descend result. Conversely, initial airspeed and flight path angle need to be increased from their present standard initial values, in order to achieve the specified values for the inertial-axis quantities.

If forward sensing is employed, an escape maneuver will be initiated earlier (i.e., at a greater distance from the microburst center) and thus the difference between the wind-axis and inertial-axis values will be smaller. Altogether, these circumstances do not make it easy to compare trajectories in different scenario's. Moreover, it is readily clear that a completely stabilized approach along the glideslope in the vicinity of a microburst, as has been assumed here, is not very realistic either. In reality the conditions at initiation of the escape maneuver are determined by (auto)pilot and (auto)throttle behavior during the glideslope approach preceding the escape maneuver. Since any choice of initial conditions apparently is somewhat arbitrary, it was decided to initially retain the standard initial conditions, and then to investigate whether modifications to the standard set of initial conditions are called for. To this end, a complementary parametric variation study involving some initial conditions has been conducted, so that particular influences on trajectory behavior could be assessed. In Ref. 13, the effects of variations in initial airspeed and throttle response have already been reported in detail. Here, the effect of variations in the initial flight path angle will be examined. Figure 5 shows the time-histories of altitude for optimal trajectories ($K_1 = 0.1$; $K_2 = 0$) that are computed based on the set of standard initial conditions, with some variations in the initial flight path angle. In addition to the standard initial value $\gamma_0 = -3°$, also $\gamma_0 = -0.5°$ and $\gamma_0 = +2°$are considered. Note that $\gamma_0 = -0.5°$ corresponds to the inertial-axis quantity $\gamma_i(0) = -3°$ in this particular scenario. The aerodynamic roll angle limit in the lateral escape procedure is 10°. Somewhat surprisingly, the value of the initial flight path angle has a rather profound impact on the transient maneuver towards the recovery altitude. However, the impact on the minimum altitude itself, as well as on the ensuing recovery procedure, is negligible. The instant at which the recovery altitude is reached is also not significantly different for the three trajectories shown. Especially note that the initial climb reemerges, in the case that a positive value of the initial flight path angle is specified, albeit on a more modest scale. In view of these findings, a new value for the initial flight path angle will be adopted for the baseline scenario for future studies, viz., $\gamma_0 = -0.5°$. Indeed, this particular

value gives a more realistic initial rate of descend in the baseline scenario, typical of a glideslope approach.

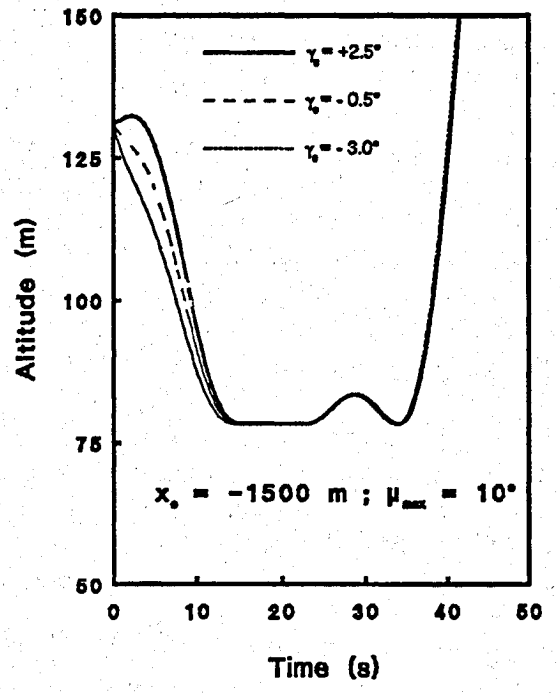

Figure 5: Comparison of extremal solutions for various values of γ_0. Lateral maneuvering, with $\mu_{max} = 10°$; weight factors $K_1 = 0.1$, $K_2 = 0$.

The baseline scenario considered thus far, considers a situation where the location of the microburst center is such that the initial conditions for the trajectories are on the maximum radial outflow velocity contour. In other words, the baseline scenario is representative of an encounter of an aircraft equipped with a reactive windshear warning system. In a scenario involving forward-look sensing, an escape maneuver is initiated earlier during the glideslope approach. More precisely, at initiation of the escape maneuver the distance between the aircraft and the microburst center is typically larger. For reasons of convenience, forward-look scenario's have been conceived here by altering the microburst location, rather than by changing the initial aircraft position. If in an open-loop optimization problem a forward-look distance R_{look} is to be simulated, the microburst center is simply displaced over a similar distance toward the runway threshold, while retaining the initial conditions.

In this Chapter some numerical results will be presented that have not been generated with the (indirect) multiple shooting approach[10], but rather with a (direct) collocation/nonlinear programming technique[13]. However, some of the direct optimization

results were validated with multiple shooting solutions. Figures 6 show some open-loop optimal Chebyshev results for a typical example in which short range forward-look sensing encounters (x_c = -1250 m) are compared with in situ (reactive) sensing encounters (x_c = -1500 m). The initial conditions are standard, including the revised initial flight path angle γ_0 = -0.5°. A forward-look detection range of 250 m is considered in this example, which features both lateral and nonturning escapes. This detection range is indeed rather short. However, it needs to be realized that longer detection ranges lead to escape trajectories that do not exhibit any altitude loss. Open-loop optimization in such a scenario is therefore pointless. On the other hand, the short range forward-look results are already sufficient to clearly demonstrate the potential performance benefits of forward look sensing.

A close examination of the results shown in Figs. 6 makes clear that lateral maneuvering is always useful, but even more so in the case of forward-look sensing. Despite the fact that only very modest banking is permitted in a lateral escape maneuver (μ_{max} = 10°), the positional advantage obtained at entry of the microburst core due to advance warning is already very significant. Although airspeed is generally higher throughout an advance warning escape (see Figure 6b), the absolute minimum speed obtained within the high-shear region (let's say, t < 40 sec.) is not significantly different for all trajectories shown.

The reason for the superior performance of advance warning escape flights is demonstrated in Figure 6c. Although only a few seconds of advance warning is considered in the present forward-look scenario, this is already sufficient to allow valuable energy to be gained before the microburst core is actually entered. In a Chebyshev solution this energy buffer is apparently used to increase the recovery altitude. Also this example shows that the rate at which specific energy is drained as a result of windshear is not notably affected by lateral maneuvering.

Figure 6d shows that due to advance warning, an escape can be commenced when the aircraft is still in the region of increasing headwind (i.e., F < 0). A negative F-factor in combination with the commanding of full throttle explains the observed initial energy increase. From Figure 6d it can also be concluded that the detection range R_{look} = 250 m corresponds to an advance warning time of 4-5 seconds. Lateral maneuvering reduces the extent of the high-shear region that is traversed, regardless whether forward looking is used or not.

Figure 6e shows the groundtracks of the two considered lateral escapes. In this particular scenario, the two groundtracks are not dramatically different. This is not really surprising, since the difference in the instances at which the aerodynamic roll angle limit leaves its limit, is about equal to the advance warning time provided by forward-look detection. However, this does not necessarily imply that lateral escapes are not at all problematic. On the contrary, if a lateral escape maneuver is commenced at a relatively large distance from the runway threshold, this will result in a large lateral offset when the y-axis is crossed. Obviously, this is far from desirable from an operational (ATC) perspective. Allowing a larger aerodynamic roll angle limit for lateral escapes may offer improved recovery altitude performance, but also aggravates the operational compatibility problems. Possibly, a scheme can be devised in which the permitted aerodynamic roll angle limit is scheduled as a function of the forward-look detection range and size of the microburst core. Moreover, it needs to be realized that once an aircraft is well past the microburst core, there is no real need to continue to steer along a wind radial. These important (operational) issues clearly need to be addressed in future research.

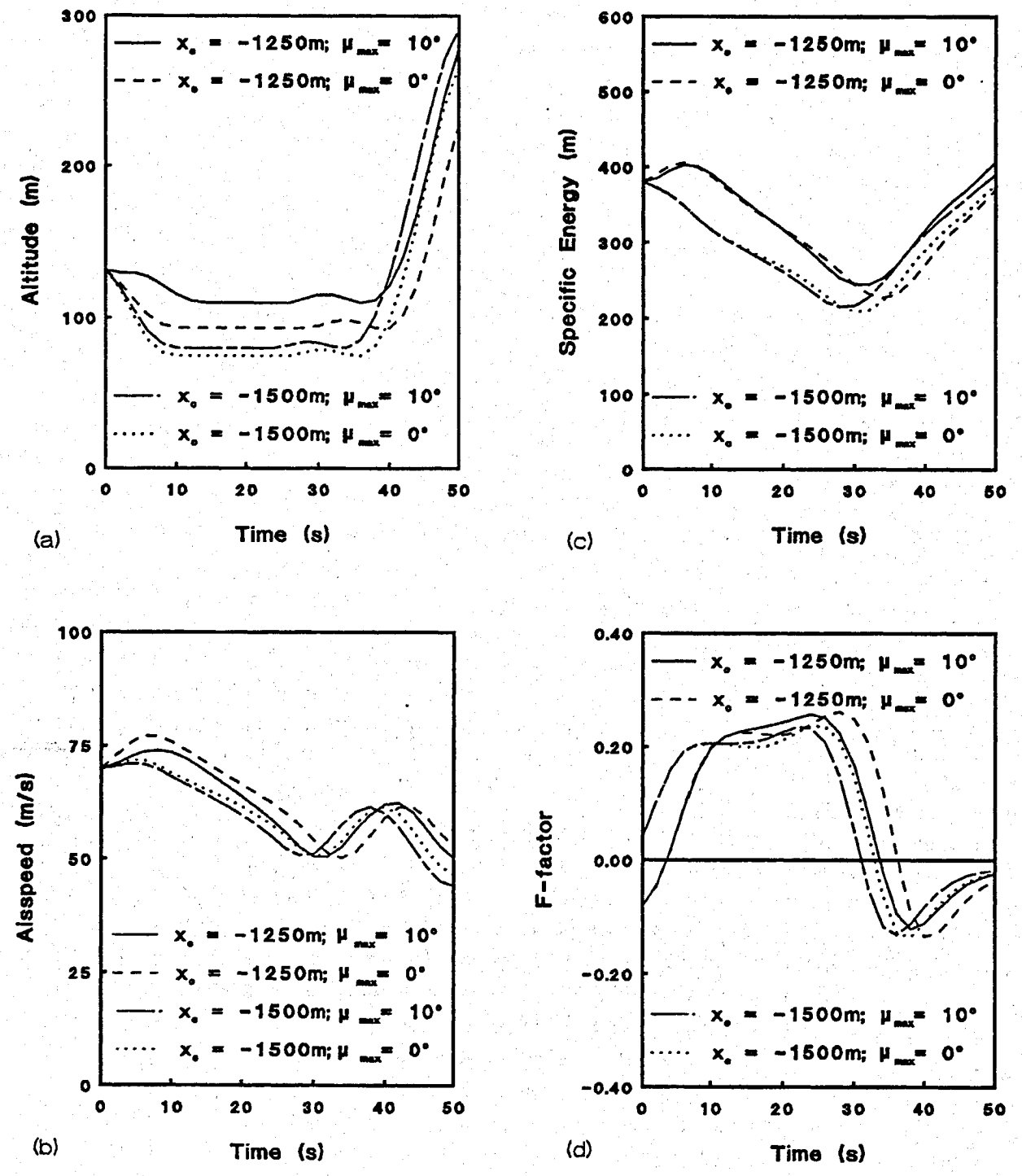

Figure 6 : Comparison of optimal Chebyshev solutions for various microburst locations x_c. Nonturning and lateral maneuvering, with $\mu_{max} = 10°$.

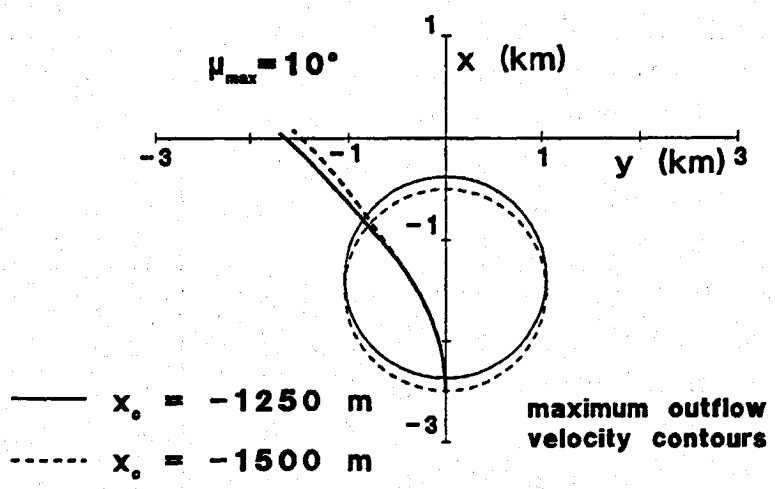

(e)

Figure 6 :
(continued)

The final numerical example involving open-loop exact solutions also concerns an early detection scenario. Similar to the previous example, the center of the microburst is located at x_c = -1250 m on the runway centerline extension. The initial conditions are almost, the same as in the previous example, except for a slightly lower initial throttle setting (which is typical for an increasing headwind situation). Also here, a lateral escape maneuver with μ_{max} = 10° is considered. The aim of this particular example is to show that the recovery altitude does not necessarily has to be much larger in a Chebyshev solution as compared with a Bolza solution. The pertinent results are shown in Figure 7. A close examination of the altitude time-histories in Figure 7 reveals that, although the Bolza and Chebyshev solutions behave very differently, the recovery altitudes are virtually the same. Also this example supports the conjecture that different guidance strategies may be employed, without incurring a significant performance penalty.

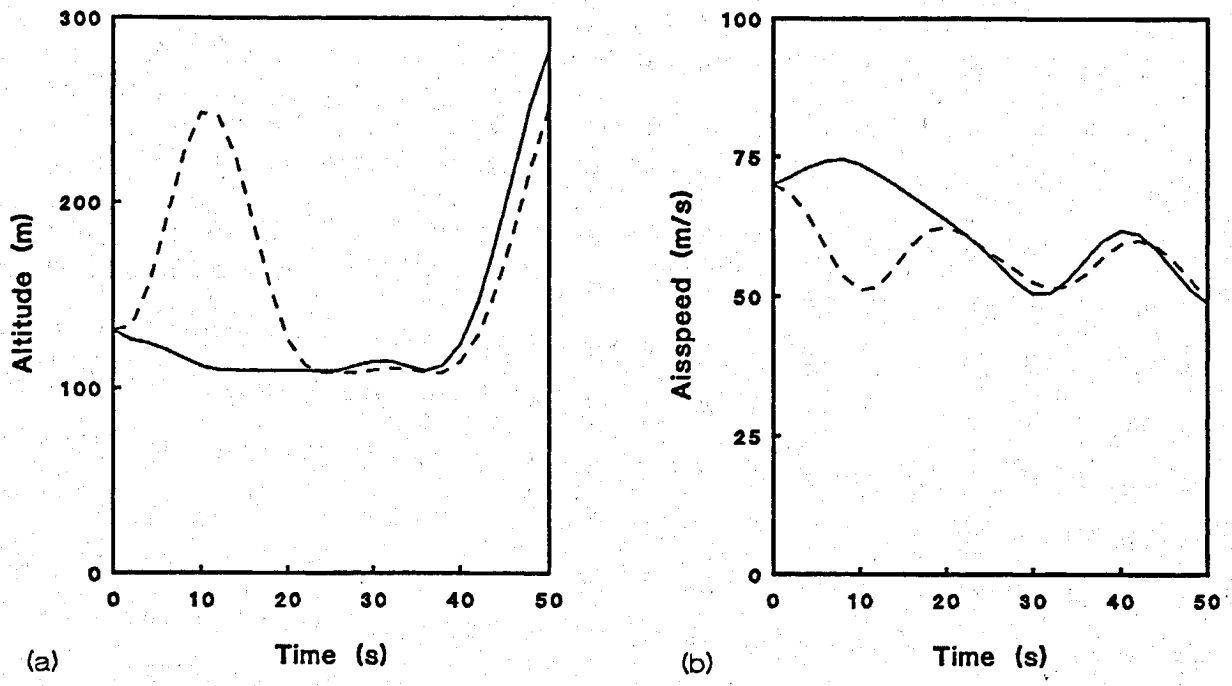

Figure 7 : Comparison of "candidate" Chebyshev solutions. Microburst location x_c = -1250m. Lateral maneuvering, with μ_{max} = 10°.

4. Closed-loop guidance approximations

In this Chapter two new longitudinal guidance laws will be derived that can possibly replace the constant pitch technique, employed in earlier work[8]. The derivation of the guidance laws closely follows the lines of Ref.11, as far as the outer control loop is concerned. The technique described in Ref.11 for synthesizing the inner control loop (for the "fast" rotational dynamics) is also very interesting and is proposed as a subject for future research. The present closed-loop guidance synthesis is based on the technique of dynamic inversion[14-20].

The essence of dynamics inversion (which is also called prelinearizing transformation technique) is to find a nonlinear transformation of variables (introduction of so-called pseudo controls), through which a nonlinear system can be transformed into a linear system. Subsequently, a relative simple control law can be developed that gives the linear system the desired characteristics, after which an inverse transformation takes place to the original variables. The method is particularly useful for determining the control input histories (feedforward control) to obtain desired outputs. This is only part of the control design, since feedback control is almost always necessary for a satisfactory implementation. However, feedback is mainly used to provide or augment stability and to handle disturbances and model inaccuracies. The output histories and the control input histories are largely determined by the feedforward logic.

The aim is to develop a closed-loop guidance scheme which approximates the open-loop optimal trajectories, by relying on local (in situ measurable) wind information only. Obviously, if global wind information (forward-look sensing) is available, more advanced schemes can be conceived that exploit this information. The constant pitch technique in conjunction with the guidance law for the aerodynamic roll angle, derived in Ref.8, is used here as a baseline scheme against which more advanced schemes can be compared. The relatively modest information set that is required for the baseline scheme can probably be obtained from in situ measurements and is therefore not likely to pose a major stumbling block for onboard implementation.

From the behavior of the optimal trajectories it was inferred in Ref.8 that the guidance law for the aerodynamic roll angle should take the following simple form:

$$\mu_c = K_\mu(\chi_w - \chi) \quad , \quad |\mu| \le \mu_{max} \quad , \tag{32}$$

with the gain coefficient K_μ selected as 0.25 and where it is understood that:

$$-180° \le \chi_w \le 180° \quad , \quad -180° \le \chi \le 180° \tag{33}$$

The guidance law for the aerodynamic roll angle attempts to close the "heading error", where heading error is defined as the relative (horizontal) wind direction. The constant pitch guidance is based on a target pitch:

$$\alpha_c = \theta_{ref} - \gamma \quad , \quad 0 \le \alpha_c \le \alpha_{max} \quad , \tag{34}$$

with θ_{ref} selected as 15°, as specified in the Windshear Training Aid (WTA)[21].

The development of the new longitudinal guidance strategies is based on an analysis involving fully coupled dynamics. However, in the derivation of the guidance laws zero sideslip angle is assumed. Also the small angle approximation has been reintroduced in the equations of motion, for the thrust vector components along and perpendicular to the airspeed vector respectively, i.e., $\cos(\alpha+\delta) \approx 1 - \frac{1}{2}(\alpha+\delta)^2$ and $\sin(\alpha+\delta) \approx (\alpha+\delta)$.

In view of the rather basic application of dynamic inversion, the description of the synthesis method will be kept brief here. The objective is to control altitude and/or climb rate by inverting the aircraft dynamics. Differentiation of Eq.(6) yields :

$$\begin{aligned} \ddot{h}(t) &= V\cos\gamma\dot{\gamma} + \dot{V}\sin\gamma + \dot{W}_h \\ &= g\left[\sin\gamma\frac{T\left[1-\frac{1}{2}(\alpha+\delta)^2\right]-D}{W} + \cos\gamma\frac{L+T(\alpha+\delta)}{W}\cos\mu - 1\right] \\ &= u_c \ , \end{aligned} \tag{35}$$

where u_c is an artificially introduced pseudo control. Observe that Eq.(35) relates u_c to a quadratic polynomial in α, which is the original control variable. Next, the form of control must be specified to obtain the desired altitude dynamics. Unlike Ref.11, where Proportional-Integral-Derivative (PID) control is used, here only P or PD control is used for the time being. The first longitudinal guidance law that we specify will be referred to as ***altitude guidance*** :

$$\ddot{h}(t) = u_c = -\left(2\zeta\omega_0\dot{h} + \omega_0^2(h - h_c)\right), \tag{36}$$

where h_c is the commanded altitude. The second longitudinal guidance law has been christened ***climb-rate guidance*** :

$$\ddot{h}(t) = u_c = -K_h(\dot{h} - \dot{h}_c), \tag{37}$$

where $\dot{h}_c$ is the commanded climb rate. By choosing the feedback gains appropriately, the altitude or climb-rate response of the aircraft can be shaped as desired, as long as no control saturation occurs. Unfortunately, however, a microburst of some significance is likely to force angle-of-attack to its maximum permissible limit, as the flight progresses.

After the pseudo control u_c has been evaluated using either Eq.(36) or (37), the result can be substituted in Eq.(35). Assuming that the aerodynamic roll angle command has been evaluated using Eq.(33), Eq.(35) allows α to be solved in closed form in terms of the state variables. Obviously, the resulting angle-of-attack command needs to be subjected to the constraint (13).

Although the control calculation steps have been determined, the question how to specify the altitude or climb-rate command still needs to be answered. At this stage, however, we prefer not to address this issue, but rather to delay the discussion to a later Chapter. The only addition to the above derivation we presently wish to make concerns the possible scheduling of the commanded climb rate in terms of an aircraft's instantaneous available climb performance. Similar to Ref.11, we propose the use following feedback scheme for the commanded climb rate :

$$\dot{h}_c = K_E\dot{E} \tag{38}$$

Recalling that the time derivative of energy can be expressed as :

$$\dot{E} = \dot{h} + \frac{V}{g}\dot{V}, \tag{39}$$

it is clear that the gain factor K_E in Eq.(38) determines how specific energy is shared between kinetic and potential energy. The selection/scheduling of the various control gains is also discussed in the next Chapter.

5. Simulated guidance solutions

A simulation program has been set up that is capable of simulating various guidance techniques or combinations of guidance techniques. In situ and/or forward-look sensing of windshear is provided, albeit in the simplified form described in Chapter 2. Indeed, the simulated windshear detection system contains two (input) parameters only, viz., the detection range R_{look}, and the F-factor detection threshold F_{thres}. An escape maneuver is initiated as soon as the measured F-value exceeds this specified threshold value. To simulate a reactive detection system, R_{look} is specified as zero (in future simulation trials possibly even slightly negative, to simulate a turbulence filter delay).

The simulation program contains a simple guidance scheme for maintaining a stabilized localizer/glide-slope approach for the flight phase prior to the windshear alert. A switch to the escape logic is made as soon as the predicted (measured) F-factor exceeds F_{thres}. This escape logic involves the lateral guidance law (32) and, by choice, one of the two longitudinal guidance laws (34), and (37), or the altitude guidance law (36), in combination with either the pitch control law (34) or the climb-rate control law (37).

Indeed, the altitude guidance law can not be utilized throughout the entire recovery maneuver. Once the high-shear region has been exited, some kind of climb scheduling is required, to move the aircraft away from its recovery altitude. Here, a switch from altitude guidance to climb-rate guidance is triggered as soon as the energy drain has been stopped, i.e, if $\dot{E} > 0$. In this study climb-rate is always scheduled in terms of the energy rate $\dot{E}$, as expressed by Eq.(38). The value of the gain factor K_E employed in the ensuing climb in the after-shear region is 0.5.

Pitch control and climb-rate control can be used for both the entry and the exit phases of the microburst encounter. In the present simulation effort pitch guidance has always been based on a 15° reference pitch angle throughout the escape flight. However, depending on the aircraft type, different values for θ_{ref} may be attempted for improved results in future research[22].

The potential advantage of the climb-rate control technique in comparison to the altitude guidance technique is that, in a certain sense, it is adaptive. The altitude guidance technique will always transfer the aircraft to the commanded altitude, regardless of the strength of the actually experienced windshear. So if, e.g., a microburst turns out to be milder than originally anticipated, the resulting specific energy savings are invested in kinetic energy, rather than in potential energy. On the other hand, if climb rate is commanded in terms of an aircraft's instantaneous available climb performance, the rate of descend will be lower in moderate windshear, than in severe windshear. Consequently, the lower the strength of the microburst, the higher the recovery altitude. Unfortunately, however, it has proved to be rather difficult to actually realize these potential benefits in a practical implementation of climb-rate guidance. As a matter of fact, without elaborate gain scheduling (K_E), climb-rate guidance is hardly useful. Preliminary experiments have revealed that it is rather difficult to come up with a single gain scheduling scheme that produces near-optimal results in a variety of scenario's (including different microburst locations and intensities, F-factor threshold values, forward-look detection range, lateral and nonturning escapes, etc.). Gain scheduling is particular difficult for the flight phase prior to entry of the microburst core, as well as in the initial descend in the core. This descend is halted as soon as the center of the microburst has been reached (i.e., the F-factor has reached a peak value), by commanding a climb rate zero ($K_E = 0$).

The climb out of the shear region is then executed by sharing energy gains equally between kinetic en potential energy (i.e., $K_E = 0.5$). In the numerical examples that we will present, the simulated climb-rate guidance solutions have all been established based on the following scheme, covering three consecutive flight phases :

- At initiation of the escape maneuver full throttle is commanded. Full throttle is maintained throughout the escape (phases 1, 2 and 3)
- In a lateral escape maneuver, the commanded aerodynamic roll angle is always calculated first (phases 1, 2 and 3).
- The commanded angle-of-attack is calculated based on the above roll angle calculation and a gain $K_E = 0.25$ if $\dot{E} > 0$ (phase 1a) and $K_E = 0.75$ if $\dot{E} < 0$ (phase 1b).
- Zero climb-rate is commanded in the core as soon as the F-Factor reaches a peak, i.e., $K_E = 0$ is set (phase 2).
- A climb out of the high-shear region is commanded as soon as $\dot{E} > 0$. The commanded climb rate is calculated based on a gain $K_E = 0.5$ (phase 3).

A few observations with regard to the above scheme are in place. Flight phase 1 covers the flight in the increasing headwind portion (just outside the peak outflow contour), as well as the forced descend in the shear region. In the region of increasing headwind (which has been labeled phase 1a), it is possible to actually gain specific energy, provided that the engines can spool up sufficiently fast. However, it turns out that it is better to use this energy to build up a speed reserve, rather than to significantly increase altitude. Indeed, simulation results bear out that if the core is penetrated at a relatively high altitude, an aircraft is exposed to a relatively large downdraft and, consequently, it will lose more energy. It needs to be noted that phase 1a can only be present in the case of a forward-look sensing scenario.

Once the energy drain starts (phase 1b), the emphasis on preserving airspeed is even reinforced by increasing the gain K_E from 0.25 to 0.75. During the resulting forced descend the F-factor is continuously monitored. If the F-factor is found not to (temporarily) increase anymore, a switch is made to zero climb rate command. This logic is based on the observation that in most scenario's Chebyshev solutions enter the minimum altitude constraint at or near the point where the F-factor starts to level off. In a real-world situation it may turn out to be rather difficult to identify this leveling off in the F-factor, since the measured F-factor signals will be blurred by the presence of high-frequency turbulence. This important issue will be discussed in the next Chapter. The zero climb-rate command is then maintained until the shear is exited (phase 2). It is important to note that altitude actually decreased during this phase 2 as a result of the fact that the climb-rate dynamics are shaped as a first-order lag. Indeed, the gain factor K_h in Eq.(37) is a very important parameter. Here, K_h has been selected as 0.25. This particular selection offers the best overall agreement of simulated guidance solutions and exact Chebyshev solutions. Increasing the value of K_h leads to a faster response, but angle-of-attack will tend to increase much quicker. This implies that the angle-of-attack limit is generally reached much earlier, possibly well before the shear region has been traversed.

If on the other hand the gain K_h is decreased, the altitude response is more sluggish and the recovery altitude is usually lower. The advantage of a low gain is that lower angles-of-attack are commanded, so that the point of control saturation can be delayed. In other words, a low gain K_h makes an aircraft less sensitive to microburst strength. Clearly, the selection of K_h represents a compromise between "performance" and "robustness'.

The present schedule for the gains K_h and K_E results in a relatively docile, but not really close to optimal behavior of climb-rate guidance. Perhaps, some slight performance improvements can still be obtained by performing a more exhaustive simulation effort, but prospects seem to be rather bleak. In contrast, altitude guidance demonstrated a better than expected behavior and performance. Also in this guidance scheme some gains need to be selected, but the overall performance turned out to be fairly insensitive to a particular choice. In the numerical examples that we will present, the following selection has been made for the coefficients in Eq.(36), $\omega_0 = 0.25$ rad/s and $\zeta = 0.8$. As already discussed in Chapter 3, the real difficulty lies in the selection of the commanded (recovery) altitude. Although the objective is to select this altitude as high as possible, based on in situ wind information only it is simply not possible to a priori predict up to which altitude a safe recovery can be made. By commanding a relatively low recovery altitude, performance is traded in favor of reduced sensitivity to the microburst strength.

To illustrate the three guidance concepts, this Chapter is concluded with some numerical examples. To allow a comparison with exact Chebyshev solutions, the same scenario's are considered as in Chapter 3 (see Figure 6). Both in situ ($R_{look} = 0$ m) and short range forward-look ($R_{look} = 250$ m) detection are considered. The value F_{thres} is taken as 0.04 for both sensors. In all scenario's the same initial condition is used, but the microburst location is 250 m displaced in longitudinal direction in the forward-look sensing scenario's. Effectively, this implies that there is no initial glideslope/localizer approach phase, but an escape commences right at the initial condition. The only reason for such a setup of the scenario's is to obtain a fair basis of comparison with the exact solutions. Included in the comparative examples, is the tradeoff of a nonturning escape versus a lateral escape ($\mu_{max} = 10°$).

In order to permit a quantitative assessment of the recovery performances of the various guidance concepts, the recovery altitudes of the exact Chebyshev solutions shown in Figure 6 are summarized in Table I.

Table I : optimal recovery altitudes of exact Chebyshev solutions in Figure 6.

	$x_c = -1250$ m	$x_c = -1500$ m
$\mu_{max} = 0°$	93.4 m	74.9 m
$\mu_{max} = 10°$	109.5 m	80.0 m

The four open-loop Chebyshev solutions shown in Table I have been approximated by simulated closed-loop guidance solutions, using the three aforementioned guidance techniques. The results are presented in Figures 8 through 11. In the early detection scenario's (x_c = -1250 m) the commanded altitude h_c = 90 m, while for the reactive sensing cases (x_c = -1500 m), h_c is taken as 70 m. In order to be honest, it needs to be admitted that the specification of the command values has been based on the exact open-loop solutions listed in Table I. If, e.g., the commanded altitude h_c = 90 m is adopted for altitude guidance in general, some serious performance penalties will be incurred. Conversely, h_c = 70 m can be specified in all scenario's, but this unnecessarily compromises the recovery altitude performance in advance warning situations.

Figures 8 show guidance solutions for escapes that are confined to a vertical plane, and for which advance warning is given. The best performance is clearly obtained with altitude guidance. Although the commanded altitude (90 m) is very close to the open-loop optimal recovery altitude (93.4 m), the altitude guidance law does not have any problem with tracking the commanded altitude, throughout the high-shear region. In contrast, the climb-rate guidance solution slightly prematurely enters the angle-of-attack limit (see Figure 8d), due a fractionally larger energy drain (see Figure 8c). These small differences are already sufficient to cause a considerable altitude drop. Nevertheless, climb-rate guidance still easily outperforms pitch guidance. The constant pitch technique is the only one that manages to avoid running into the angle-of-attack limit. Consequently, higher speeds (see Figure 8d) can be maintained throughout the escape. This fact, combined with the fact that the overall energy loss is largest for pitch guidance, results in a rather severe penalty on recovery altitude. The time-history of angle-of-attack for climb-rate guidance exhibits a seemingly peculiar instantaneous jump. This jump is caused by gain scheduling. More specifically, it is the result of setting K_E = 0 (down from K_E = 0.75) near the center of the microburst. Lateral behavior is not very different for the three guidance techniques and is therefore not shown here.

Figures 9 are based on the same scenario as Figs. 8, but this time lateral escapes are considered. All three guidance techniques now result in a markedly better performance, not only in terms of recovery altitude, but also in terms of (lowest) airspeed. Due to the short-cut within the high-shear region, less energy is lost and, consequently, all three techniques manage to avoid reaching the stick shaker limit. In comparison with the corresponding nonturning escape, climb-rate guidance benefits relatively the most, as it leads to the highest recovery altitude. However, we would not like to go as far as to qualify climb-rate guidance as the "winner" in this particular scenario. The reason for this is that, as we will see, it is still possible to command a higher recovery altitude for the altitude guidance technique. A comparison between Figure 9a and Figure 6a reveals that the climb-rate guidance solution is in close agreement with the exact open-loop solution, as far the initial stage is concerned, yet the difference in recovery altitude is eventually still considerable.

Escape solutions obtained in the absence of early warning are shown in Figure 10 (nonturning escapes) and Figure 11 (lateral escapes), respectively. It can be observed that the differences between altitude guidance and climb-rate guidance are not large in this scenario. Although lateral maneuvering still leads to an increase in recovery performance, the improvements are not nearly as impressive as in the case of advance warning, at least for climb-rate guidance. For the constant pitch technique, the improvement in recovery altitude due to lateral maneuvering is still significant (about 10 m).

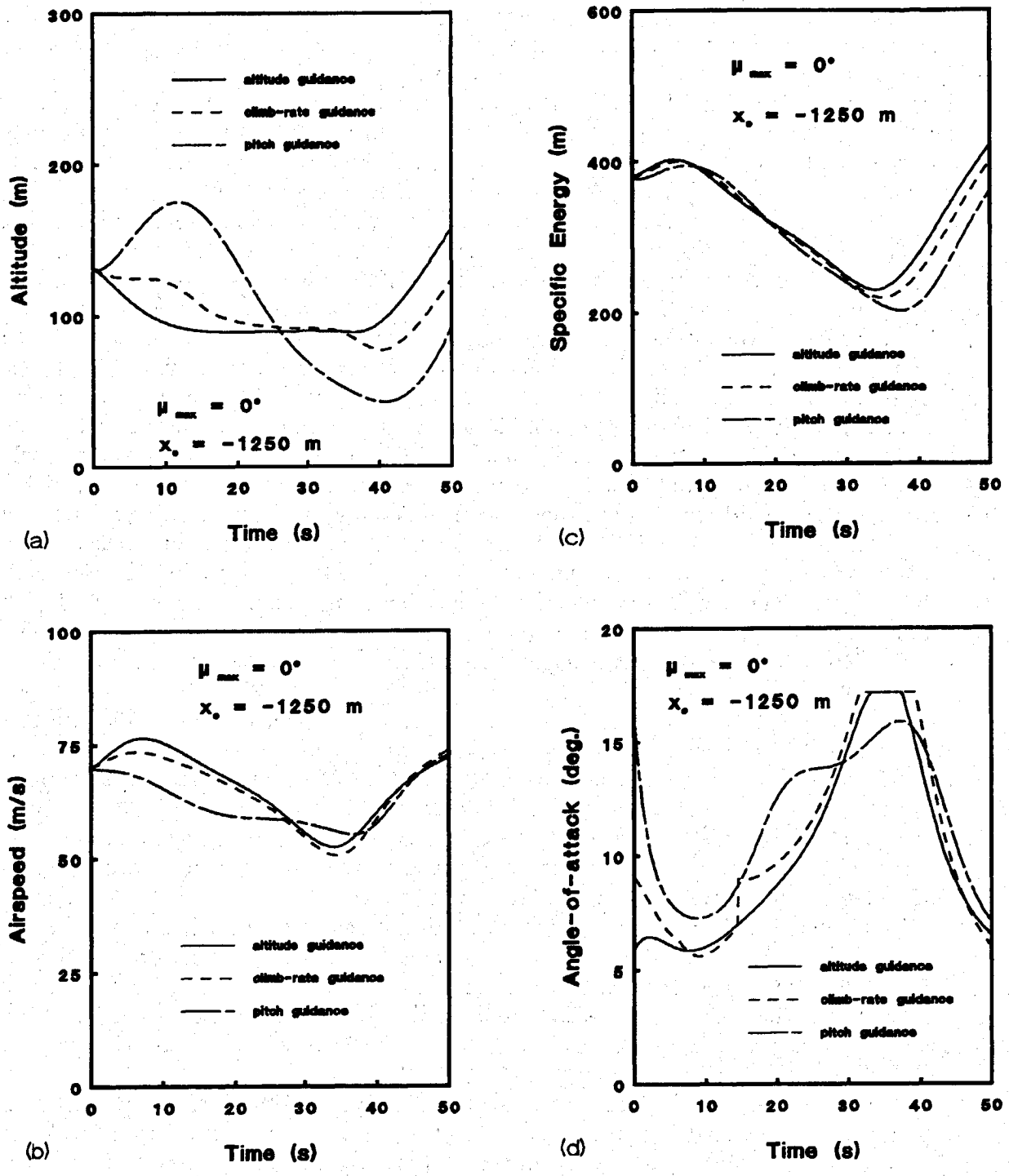

Figure 8 : Comparison of various simulated guidance solutions for a microburst location x_c = -1250 m. Nonturning escapes (μ_{max} = 0°).

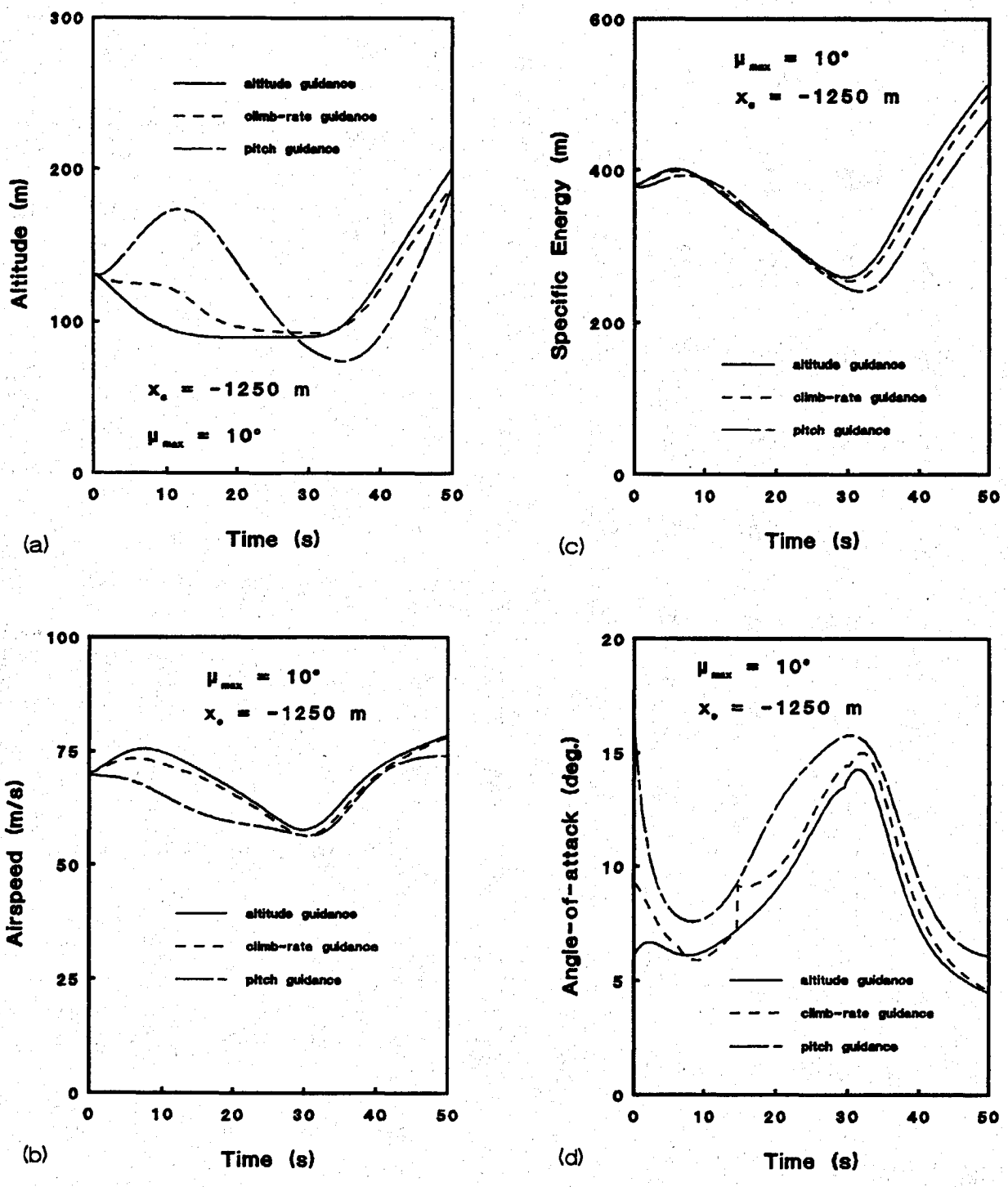

Figure 9 : Comparison of various simulated guidance solutions for a microburst location x_c = -1250 m. Lateral escape maneuvers (μ_{max} = 10°).

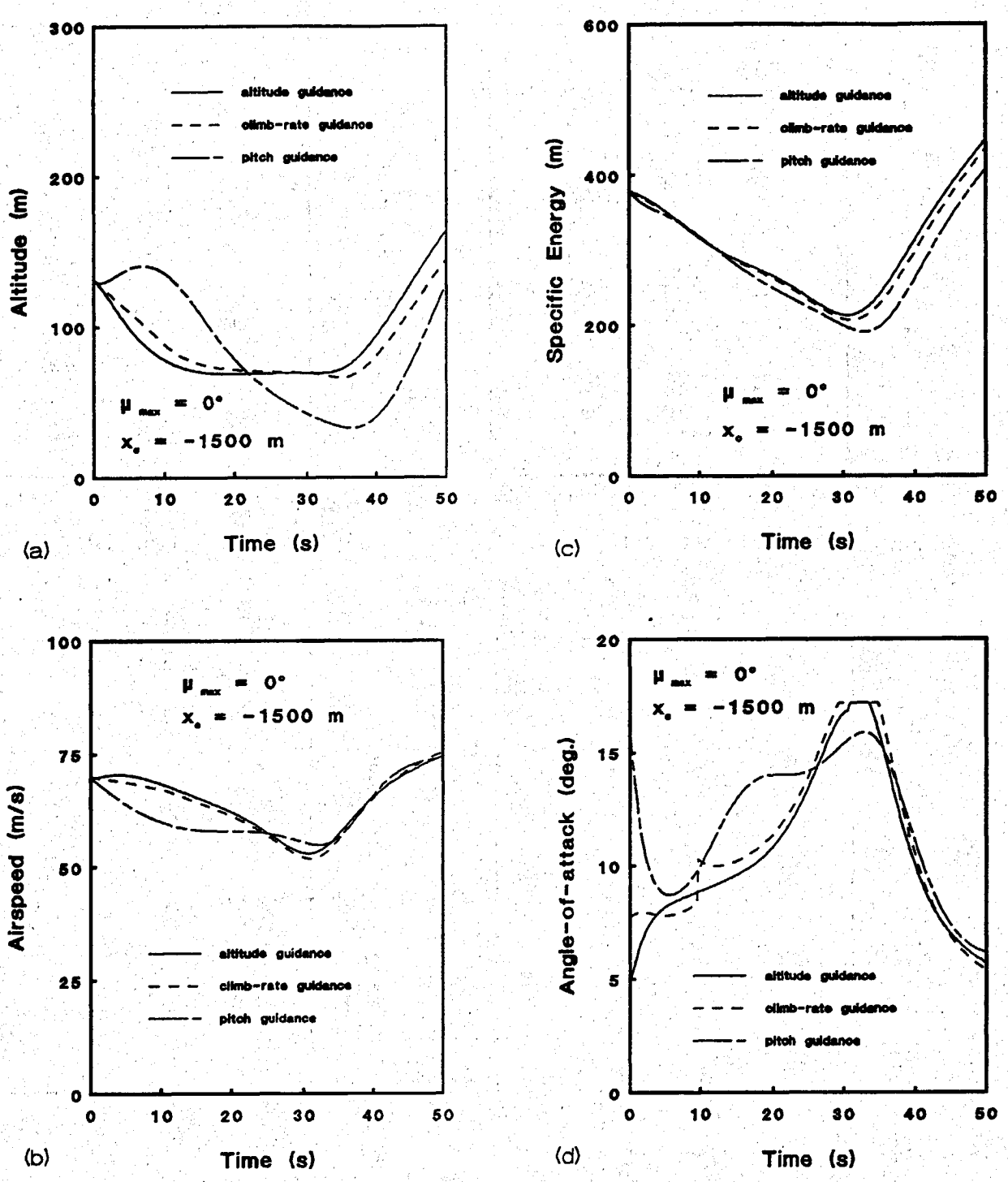

Figure 10 : Comparison of various simulated guidance solutions for a microburst location x_c = -1500 m. Nonturning escapes (μ_{max} = 0°).

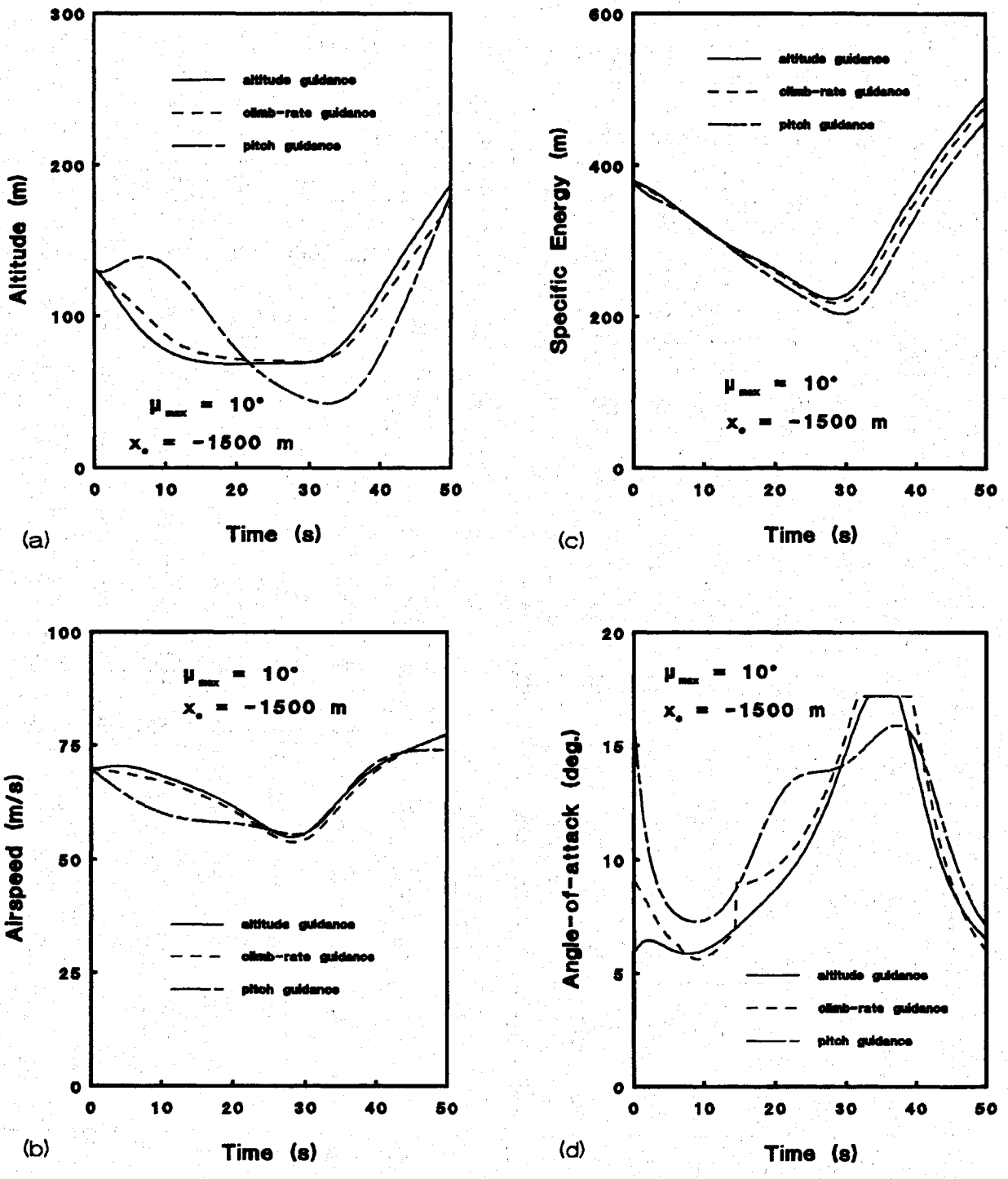

Figure 11 : Comparison of various simulated guidance solutions for a microburst location x_c = -1500 m. Lateral escape maneuvers (μ_{max} = 10°).

The final guidance example involves altitude guidance only. The considered scenario is exactly the same as in Figures 8 and 9, but now the commanded altitude h_c has been increased from 90 to 100 m. Inspection of Table I learns that a recovery altitude of that magnitude is ideally achievable for a lateral escape, but not for a nonturning escape. The results for the nonturning and lateral escapes are shown in Figure 12. For illustrative purposes, a lateral escape with a slightly larger aerodynamic roll angle limit has been included (μ_{max} = 15°). The effect of the increased commanded altitude is readily apparent. Without lateral maneuvering, the airspeed reserve is insufficient to withstand the energy drain due to windshear, and the commanded altitude can not be maintained throughout the encounter. The lateral escapes, however, succeed well in limiting the energy loss and as a result, recovery can take place at the desired altitude. Executing a lateral escape with a higher aerodynamic roll angle limit results in an even better management of specific energy.

Based on the simulation experiments, we feel that altitude guidance is the most promising of the three concepts, in terms of performance and robustness characteristics. Moreover, this simple technique is probably readily accepted by pilots, especially when short range forward-look sensing is employed. In contrast to the constant pitch technique, there are no dramatic altitude excursions during the escape maneuver. Such excursions tend to raise the anxiety levels of pilots[6].

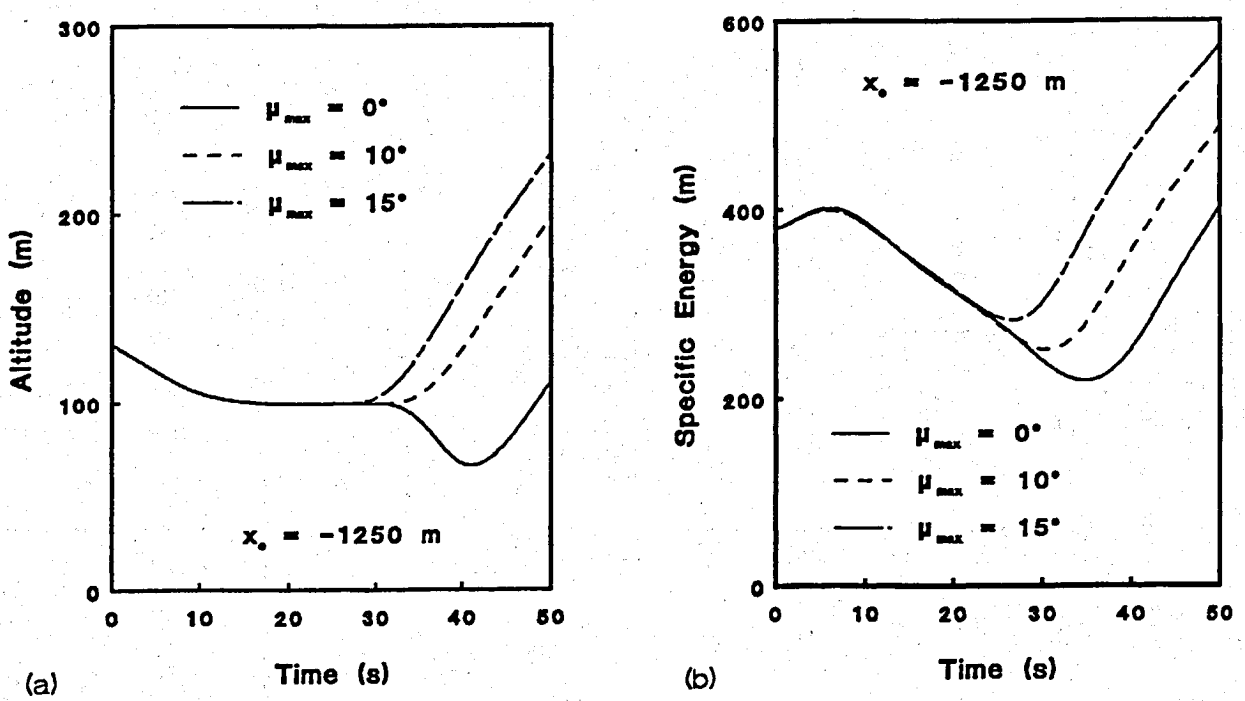

Figure 12 : Comparison of simulated altitude guidance solutions for several values of the aerodynamic roll angle limit. The microburst is located at x_c = -1500 m. The commanded recovery altitude h_c = 100 m.

The only real problem remaining that needs to be solved before a practical implementation of altitude guidance can take place is the development of the logic for determining the attainable recovery altitude. The development of such logic for application in a closed-loop guidance scheme is conceivable, if it is possible to make a realistic estimation of the total windshear induced energy loss. If a long range forward sensor is used (capable of probing the overall extent of the microburst), such an estimation is perhaps possible. However, as already mentioned before, if long range advance warning is available, there is no real need for escape guidance, as the microburst can be completely avoided through the execution of a standard go around. When short range forward-look sensing is used, it is perhaps possible to relate the commanded recovery altitude to the energy gain prior to core penetration, and/or to adapt the commanded altitude as the recovery unfolds. In any case it is clear that much further research is needed to develop this type of intelligent controller.

6. Wind and windshear measurement

In this Chapter we will briefly assess the availability and quality of the information used in the various state feedback guidance schemes. In particular, the real-time identification of wind related quantities, such as the F-factor and the relative wind direction, will be investigated. The sensors to measure the required information may include the usual air data instruments and inertial sensors (IRS), as well as advanced systems for predictive detection and warning (like lidar or radar).

The three different longitudinal escape guidance laws have different sensor requirements. However, all three are triggered by the (estimated) F-factor exceeding the specified threshold value F_{thres}. The climb-rate guidance law also uses the F-factor to schedule the feedback gains. Ergo, the F-factor needs to be estimated onboard. References 1 through 6 discuss the real-time F-factor estimation in great detail, for both reactive and predictive systems. For this reason, the discussion on the F-factor calculation will be kept rather brief here. Unlike the constant pitch guidance law, which is rather easy to evaluate, the climb-rate and altitude guidance laws are somewhat complex in terms of the feedback/feedforward information. The feedforward term (see Eq.(35)) contains such hard to estimate quantities as gross weight, thrust, lift and drag. However, we do not expect that estimation inaccuracies are likely to have a strong influence on the guidance performance[23]. Obviously, any simplification of the guidance laws needs to be validated through extensive simulation. It is important to note that none of the proposed longitudinal guidance laws explicitly contains wind terms. Indeed, the effects of shear and downdraft are all combined in a single entity, the F-factor. Consequently, there is also no real need to estimate the individual wind components.

The longitudinal guidance laws also feature switches and gain schedules based on the total rate of change of specific energy, $\dot{E}$. Moreover, the commanded climb-rate is scheduled in terms of $\dot{E}$ in the climb-rate guidance law. Fortunately, this quantity can be measured directly using total energy-rate sensors[24]. At this stage it is not clear whether measuring the total energy-rate is really necessary for altitude guidance. However, the availability of this information could certainly aid the development of logic for determining the commanded recovery altitude.

The lateral guidance law (32) is based on the feedback of the relative wind direction. In this Chapter we will assess whether it is possible to estimate the horizontal wind direction from in situ and/or short range forward-look sensing of windshear. If long range forward-look sensing is employed, it is probably possible to determine the approximate location of the microburst center, with some accuracy. In that case the wind direction can be "computed" by simply determining the line-of-sight angle from any given aircraft position (see Figure 2). However, we have to remain aware of the fact that in the simulations highly "idealized" windshear models are used. In a real-world situation the actual characteristics of a microburst may be more complex than that of a basic model featuring a single downburst center. Consequently, in reality spatial wind variations will generally exhibit a far more erratic behavior than the simple models suggest.

At first glance, it may appear that the estimation of the relative wind direction is not very critical. In the initial headwind phase, prior to entry of the core, the relative wind angle will be usually so large that the guidance law (32) will call for maximum aerodynamic roll angle. Moreover, simulation experiments have shown that the performance solution is not very sensitive with respect to debanking behavior either. What is important is that the aircraft does not make a turn in the wrong direction, i.e., a turn towards the microburst center. As already shown in Ref. 8, turning in the wrong direction may have dramatic consequences with respect to the recovery altitude. The scenario's considered in this report all assume a symmetric encounter and therefore it makes no difference whether a left or a right turn is executed. When, however, the center of the microburst is laterally offset from the runway centerline extension, the choice of turn direction becomes important. The turn should always be executed in the same direction as the (mean) crosswind is blowing. The stronger the experienced crosswind component, the more critical it is that the choice of turn direction is correct. It can thus be concluded that the relative wind direction must be estimated with some degree of accuracy. The question is whether in a real-world situation the estimated wind direction (or wind vector components) is not too much corrupted by high-frequency turbulence signals. Although we will not make an attempt to truly answer this and similar questions, we will briefly outline an onboard data processing procedure for computing the F-factor and the wind vector, primarily to identify potential sources of problems.

It is assumed that the following quantities can be measured onboard, ambient pressure p_a, ambient temperature T_a, indicated airspeed V_{IAS}, angle-of-attack α, sideslip angle β, acceleration components (in body axes system) a_{bx}, a_{by}, a_{bz}, yaw angle ψ, pitch angle θ and roll angle ϕ. In case sideslip is not explicitly measured, this quantity can be indirectly computed using the procedure described in Ref.3. Some quantities that are easily derived from these measurements include airspeed V, (barometric) altitude h, and air density ρ. For other variables, the pertinent conversion formulae may be more complicated. The equations of motion (4) through (9) are written in terms of the wind-axes variables. These wind-axes quantities can be readily related to the measured quantities by factorizing the wind-to-Earth frame transformation matrix L_{EW}[3] :

$$L_{EW} = L_{EB} \cdot L_{BW} \,, \tag{40}$$

where L_{EB} is the body-to-Earth frame transformation matrix, and L_{BW} is the wind-to-body frame transformation matrix. Equating left- and righthand sides of Eq.(40) yields the following relations :

$$\tan\chi = \left[(\cos\alpha\cos\beta)(\cos\theta\sin\psi) + (\sin\beta)(\sin\phi\sin\theta\sin\psi + \cos\phi\cos\psi) + (\sin\alpha\cos\beta)(\cos\phi\sin\theta\sin\psi - \sin\phi\cos\psi)\right] / \left[(\cos\alpha\cos\beta)(\cos\theta\cos\psi) + (\sin\beta)(\sin\phi\sin\theta\cos\psi - \cos\phi\sin\psi) + (\sin\alpha\cos\beta)(\cos\phi\sin\theta\cos\psi + \sin\phi\sin\psi)\right] \quad (41)$$

$$\sin\gamma = (\cos\alpha\cos\beta)(\sin\theta) - (\sin\beta)(\sin\phi\cos\theta) - (\sin\alpha\cos\beta)(\cos\phi\cos\theta) \quad (42)$$

$$\tan\mu = \frac{(\cos\alpha\sin\beta)(\sin\theta) + (\cos\beta)(\sin\phi\cos\theta) - (\sin\alpha\sin\beta)(\cos\phi\cos\theta)}{(\sin\alpha)(\sin\theta) + (\cos\alpha)(\cos\phi\cos\theta)} \quad (43)$$

From Eqs.(4) through (6) the wind vector can be computed as :

$$W_x = \dot{x} - V\cos\gamma\cos\chi \quad (44)$$

$$W_y = \dot{y} - V\cos\gamma\sin\chi \quad (45)$$

$$W_h = \dot{h} - V\sin\gamma \quad (46)$$

Taking the total time derivatives of Eqs.(44) through (46) yields :

$$\dot{W}_x = \ddot{x} - \frac{d}{dt}(V\cos\gamma\cos\chi) \quad (47)$$

$$\dot{W}_y = \ddot{y} - \frac{d}{dt}(V\cos\gamma\sin\chi) \quad (48)$$

$$\dot{W}_h = \ddot{h} - \frac{d}{dt}(V\sin\gamma) \quad (49)$$

The above time derivatives of the wind vector are needed to evaluate the expression for the F-factor, which is found by substituting Eq.(7) into Eq.(21) :

$$F = \frac{1}{g}[\dot{W}_x \cos\gamma\cos\chi + \dot{W}_y \cos\gamma\sin\chi + \dot{W}_h \sin\gamma] - \frac{W_h}{V} \tag{50}$$

Substitution of Eqs.(46) through (49) into Eq.(50 yields :

$$F = \frac{1}{g}[\ddot{x}\cos\gamma\cos\chi + \ddot{y}\cos\gamma\sin\chi + \ddot{h}\sin\gamma - \dot{V}] - \frac{\dot{h} - V\sin\gamma}{V} \tag{51}$$

The earth-fixed (inertial) accelerations are obtained from the accelerations measured in the body reference frame :

$$\begin{pmatrix} \ddot{x} \\ \ddot{y} \\ \ddot{z} \end{pmatrix} = L_{EB} \begin{pmatrix} a_{xb} \\ a_{yb} \\ a_{zb} \end{pmatrix} ; \quad \ddot{h} = -\ddot{z} \tag{52}$$

The instantaneous IRS sensor signals (accelerometers and gyro's) need to be filtered before they are fed to the detection and guidance systems. The reason for this is that the inertial measurements are contaminated with high-frequency atmospheric turbulence signals. A frequently employed way of filtering turbulence in the high frequency spectrum is to average the F-factor over a specified time-interval τ. More specifically, the average F-factor is defined as :

$$F_{av}(t) = \frac{1}{\tau}\int_{t-\tau}^{t} F\,dt \tag{53}$$

If the averaging time τ is sufficiently large, the high-frequency turbulence are filtered out. However, if τ is too large F_{av} which represents the true windshear (low-frequency spectrum) also tends to vanish. Therefore, τ must be selected judiciously, generally based on extensive experimentation.

A comparison of the F-factor histories of the simulation experiments with those of actual measurements[3] shows that the clarity of a typically averaged F-factor signal is still blurred by turbulence, resulting in many small (local) peaks superimposed on the mean wind peaks. Obviously, this may easily lead to undesirable nuisance warnings. With respect climb-rate guidance, the presence of free-stream turbulence will probably make it difficult to determine in real-time the peaks in the F-factor due to true windshear. At this point, we do not know whether it is possible to significantly improve the situation by combining in situ measurements with short-range forward-look measurements. This represents an important issue in future research. Clearly, the characteristics of the various forward-look sensor systems will need to be considered in such a study.

The in situ determination of the wind direction is probably even more problematic. In order to determine the wind direction, it is required to estimate the horizontal wind components. From Eqs.(44) through (46) it can be seen that this boils down to estimating the components of the groundspeed vector (airspeed and other air data are readily available). This calls for more advanced prediction techniques than simply averaging the measured F-factors. Several techniques have been proposed[25,26] which promise accurate estimates of wind components as well as their time derivatives, from the output of in situ sensors. With the measured wind components available, the wind direction can be directly computed from Eq.(18) :

$$\tan\chi_w = \frac{W_y}{W_x} \tag{54}$$

Also here, it is not readily apparent whether short range forward-look sensing will be all that helpful in improving the quality of the wind direction estimate. The primary reason for this concern is that forward-look sensors typically measure wind speed variations along the line-of-sight. This implies that, while such systems are capable of producing fairly good longitudinal wind predictions, they are actually limited in their capability to predict both vertical and lateral wind variations. Since lateral escape procedures have not been widely investigated, it is even doubtful whether the measurement of lateral wind variations has been examined at all.

Another real concern that has not yet been addressed relates to the (hopefully rare) occurrence of several neighboring microbursts, possibly in different stages of their development (temporal wind variations). Indeed, the in situ detection of a microburst may trigger a lateral escape, only to find out that the aircraft is turning towards the center of a second perhaps even stronger microburst located slightly further down the approach route. Of course, an optimistic scenario, e.g. escaping from one microburst while avoiding another in the process, is just as probable, but this does not take away the fact that we do not wish the outcome of the encounter to be determined by chance. An investigation of detection and guidance in a complex wind flow field is clearly warranted, obviously with due consideration to the probability of occurrence of such events.

Up to this point, we have only discussed airborne windshear detection and warning. Ground-based sensors are perhaps just as viable, particularly in view of the total system cost to the overall air transport community. Indeed, ground-based windshear detection is likely to play a large role in near-term windshear alerting and recovery and avoidance systems. Doppler radars are becoming available that are capable of detecting downbursts that impact the ground, throughout the terminal area. The ground-derived windshear information will need to be transmitted to the aircraft over a digital ground-to-air datalink (notably, mode-S). Once this technology is in place, the next step will be the fusion of ground-derived data with airborne sensor measurements. The possible outcome of these efforts is as yet unclear, but is likely to have a great impact on the development of avoidance and escape guidance strategies. For the time being, operational issues, such as compatibility with ATC procedures, will therefore not be addressed.

7. Conclusions and recommendations for future research

In this report a preliminary study on the development of a new microburst escape guidance strategy has been presented. Three different candidate laws for longitudinal guidance have been examined, in conjunction with a single lateral guidance law. In the simulated guidance solutions, the availability of perfect mean wind information (free of turbulence) was assumed. Both in situ (reactive) and short range forward-look (predictive) sensing of windshear was simulated. Based on a comparison with exact Chebyshev solutions, altitude guidance emerged as the most promising longitudinal guidance strategy. The lateral escape strategy, though very simple, proved to be very effective. The simulation results confirmed the earlier observations that a lateral escape is particularly effective in improving the recovery performance, if advance warning is provided. It can thus be concluded that by permitting lateral escape strategies, forward-look sensor requirements can be reduced so that predictive systems may become economically feasible for a much broader class of aircraft types.

Altitude guidance was shown to be fairly robust to uncertainty in the microburst strength, without any real sacrifices in terms of recovery altitude. However, a predictive logic for determining the "best" recovery altitude is an important element that is still missing. Such logic critically depends on the advance warning time and the associated ability to build up a speed buffer prior to entering the core. Another factor on which this logic will be based is the capability to predict the overall energy-loss that will be accumulated while passing through the microburst core. In this respect, the detection range and the quality of the sensor measurements will be paramount factors. The development of appropriate logic for the determining the recovery altitude is the first step to be taken, before the practicality of the altitude guidance technique can be further assessed.

One of the main reasons for undertaking the present research effort was to make an initial attempt to bridge the gap between the earlier "academic" open-loop optimization studies and more realistic (operationally oriented) piloted simulation evaluations. However, an "intermediate" (batch simulation) development step is still required, before actual piloted simulations can take place. This intermediate step does not only entail the development of missing elements, such as the logic for determining the recovery altitude, but also the refinement of existing models, such as the incorporation of the aircraft rotational inertia in both roll and pitch. More specifically, the basic point-mass vehicle model needs to be extended to a full six degrees-of-freedom (6-DOF) system model, such as to find out to what extent the advantages of the lateral escape vis-a-vis the longitudinal escape can be preserved in real-world conditions. Such a 6-DOF model allows the rolling and pitching tendencies resulting from (cross) wind variations to be studied. In addition, it provides a suitable environment for the preliminary assessment of the operational consequences of the proposed detection and guidance strategy (the impact of various maximum roll angle limits, the impact of different sensors, etc.). The sequential dynamic inversion technique provides a convenient framework for extending the point-mass modeled simulation to 6-DOF. Using this technique, an additional inner control loop can be synthesized to handle the fast time-scale rotational dynamics (short-period mode), without having to modify the outer control-loop (phugoid mode).

It can be concluded that a lateral escape strategy in combination with altitude guidance constitutes an attractive candidate for operational assessment in a piloted simulation, provided that the observed performance and robustness characteristics can be validated by high-fidelity 6-DOF batch simulation experiments.

References

1. Bracalente, E.M., and Jones, W.R., "Airborne Doppler Radar Detection of Low Altitude Windshear", *Journal of Aircraft*, Vol.27, No.2, 1990, pp. 151-157.
2. Bowles, R.L., "Reducing Windshear Risk Through Airborne Systems Technology", Proceedings of the 17th ICAS, Stockholm, 1990, pp. 1603-1630.
3. Miele A., Wang, T. and Melvin, W.W., "Advanced Windshear Detection Technique", Rice University, Aero-Astronautics Report, No. 257., 1991.
4. Hinton, D.A. "Forward-Look Wind-Shear Detection for Microburst Recovery", *Journal of Aircraft*, Vol.29, Jan.-Feb. 1992, pp. 63-66.
5. Vicroy, D.D., "Microburst Vertical Wind Estimation from Horizontal Wind Measurements", NASA TP-3460, December 1994.
6. Rouwhorst, W.F.J.A., Haverdings, H., Huynh, H.T., Descatoire, F., König, R., "Experimental Design and Testplan for a Piloted Investigation of : A Flight-Director Go-Around Mode, a Reactive Windshear Detection System, a Forward-Looking Windshear Detection System and a Windshear Display, on the NLR Research Flight Simulator", Report NLR CR95350 L, 1995.
7. Phillips, E.H., "Crash Probe Focuses on Severe Microburst", *Aviation Week & Space Technology*, September 26, 1994.
8. Visser, H.G., "Optimal Lateral Escape Maneuvers for Microburst Encounters During Final Approach", Delft University of Technology, Report LR-691, July 1992.
9. Visser, H.G., "A Minimax Optimal Control Analysis of Lateral Escape Maneuvers for Microburst Encounters", Delft University of Technology, Memorandum M-713, Nov. 1995.
10. Grimm, W., Berger, E. and Oberle, H.J., "Benutzeranleitung fur das Rechenprogram BNDSCO zur Lösung Beschrankter Optimaler Steuerungsprobleme", DFVLR-Mitt. 85-05, 1984.
11. Mulgund, S.S. and Stengel, R.F., "Aircraft Flight Control in Wind Shear Using Sequential Dynamic Inversion", *Journal of Guidance, Control, and Dynamics*, Vol.18, No.5, Sept.-Oct. 1995, pp. 1084-1091.
12. Zhao,Y. and Bryson, A.E., "Optimal Paths Through Downbursts", *Journal of Guidance, Control, and Dynamics*, Vol.13, Sept.-Oct. 1990, pp. 813-818.
13. Bruin, P.J. de, "Improved Models for Optimal Abort Landing Maneuvers in the Presence of Windshear", Thesis, Faculty of Aerospace Engineering, Delft University of Technology, August 1995.
14. Menon, P.K.A., Badgett, M.E. and Walker, R.A., "Nonlinear Flight Test Trajectory Controllers for Aircraft," *Journal of Guidance, Control, and Dynamics*, Vol. 10, No. 1, 1987, pp. 67-72.
15. Hunt, L.R., Su, R. and Meyer, G., "Global Transformations of Nonlinear Systems," *IEEE Transactions on Automatic Control*, Vol. AC-28, 1983, pp. 24-31.
16. Isodori, A., "Nonlinear Control Systems: an Introduction," *Lecture Notes in Control and Information Sciences*, Springer Verlag, Berlin, 1985.
17. Meyer, G. and Cicolani, L., "Applications of Nonlinear Systems Inverses to Automatic Flight Control Design - System Concept and Flight Evaluations," in : *AGARDograph 251* (P. Kent, ed.), 1980.

18. Azam, M. and Singh, S.N., "Invertibility and Trajectory Control for Nonlinear Maneuvers of Aircraft," *Journal of Guidance, Control, and Dynamics*, Vol.17, No.1, 1994, pp.192-200.
19. Lane, S.H., and Stengel, R.F., "Flight Control Design Using Nonlinear Inverse Dynamics," *Automatica*, Vol.24, No.4, 1988, pp.471-484.
20. Snell, A.S., Enns D.F. and Garrard, W.L., "Nonlinear Inversion Flight Control for a Supermaneuverable Aircraft," *Journal of Guidance, Control, and Dynamics*, Vol. 15, No. 4, 1992, pp. 976-984.
21. *Windshear Training Aid*, U.S. Department of Transportation, Federal Aviation Administration, Washington D.C., 1987.
22. Mulgund, S.S. and Stengel, R.F., "Target Pitch Angle for the Microburst Escape Maneuver", *Journal of Aircraft*, Vol.30, No.6, Nov.-Dec. 1993, pp. 826-832.
23. Visser, H.G. ,"A 4-D Trajectory Optimization and Guidance Technique for Terminal Area Traffic Management", Report LR-769, TU-Delft, June 1994.
24. Ostroff, A.J., et al., "Evaluation of a Total Energy-Rate Sensor on a Transport Airplane", NASA TP-2212, 1983.
25. Mulgund, S.S. and Stengel, R.F., "Optimal Nonlinear Estimation for Aircraft Flight Control in Wind Shear", *Automatica*, Vol.32, No.1, 1996, pp. 3-13.
26. Miele, A., Wang, T. and Melvin, W.W., "Real-Time Wind Identification Technique", Rice University, Aero-Astronautics Report, No. 256., 1991.
27. Wanke, C., Hansman, R.J., "Hazard Evaluation and Operational Cockpit Display of Ground-Measured Windshear Data", *Journal of Aircraft*, Vol.29, No.3, May-June 1992.